Universidade de Lisboa
Faculdade de Ciências

Departamento de Engenharia Geográfica, Geofísica e Energia

Exploring RTTOV to retrieve Land Surface Temperature from a geostationary satellite constellation

Virgílio Alexandre da Silva Marques Bento

Dissertação

Mestrado em Ciências Geofísicas

(Meteorologia)

2013

Universidade de Lisboa
Faculdade de Ciências

Departamento de Engenharia Geográfica, Geofísica e Energia

Exploring RTTOV to retrieve Land Surface Temperature from a geostationary satellite constellation

Virgílio Alexandre da Silva Marques Bento

Dissertação

Mestrado em Ciências Geofísicas

(Meteorologia)

Orientadores: Doutora Isabel F. Trigo e Prof. Doutor Carlos da Camara

2013

Agradecimentos

Tudo o que nesta tese foi escrito (e não foi) é resultado de bastantes meses de trabalho, por vezes árduo, por vezes relaxado, mas sempre e indubitavelmente rico em matéria devota a marchar contra a minha própria ignorância. Pois, verdade seja dita, o que de novo aprendi bate sem vias de dúvida o que de novo não aprendi, ou o que de velho desaprendi. Toda esta matéria, e por conseguinte todo este trabalho, bem como a referida míngua de ignorância do seu autor (mas não o seu desaparecimento), deveu-se à existência e paciência de um número de pessoas, a quem esta página, por via de mim, tem como objectivo agradecer.

À Doutora Isabel Trigo, muito tenho a agradecer. Pouco nos vimos, resultado dos quilómetros que separam o IDL do IPMA, mas esse pouco em muito se transforma, quando temos em conta a excelente orientação, a paciência e o tempo, que apesar de ser muito pouco, resultante dos seus próprios afazeres, foi de uma qualidade para além do que as palavras podem descrever. Por tudo isso e muito mais aqui fica o meu agradecimento.

Ao Professor Doutor Carlos da Camara, entre rixas desportivas, discussões literárias, muita organização desorganizada (ou desorganização organizada), risadas bem passadas e todas as variadas palavras trocadas, quero agradecer-lhe por sempre ter acreditado que, apesar de toda a aparente ignorância que este humilde e autodestrutivo súbdito demonstrou, existia algo mais escondido que nem ele próprio acreditava. Se acertou ou não, ainda está para ser demonstrado. Ao professor CC (reflexo romano de sua idade) por tudo o que fez por mim e por me ter ensinado a resolver raízes quadradas "*a la pata*" agradeço-lhe, e espero um dia, quando for o professor CCC de bengala e a babar-se, poder continuar a agradecer-lhe por novos ensinamentos.

Aos três da vida airada, Daniela, Maria João e Jorge, por me terem ajudado sempre que necessário, com grandes almoçaradas, jantaradas, cinemas, passeios, maluquices, discussões de culturais a supérfluas. Agradeço-vos por todas as festas que fizemos, no decorrer da minha, e também das vossas teses: à Maria João por ser a primeira a largar tudo e festejar comigo qualquer coisa, com ou sem sentido (mais sem do que com); ao Jorge pelas discussões literárias, desportivas ou piscatórias; mas em especial à Daniela por me ter aturado mais de perto e, como única mente responsável entre as 8h e as 18h, me tenha chamado à razão da minha enorme inconsciência e displicência, quando necessário.

Aos meus pais, por me terem sempre incentivado a ir para a frente e nunca desistir, por me terem aturado nos dias maus e nos dias bons. Por terem sido um porto seguro, um chamamento de razão e estarem em constante gozo e brincadeira comigo, vos agradeço.

Abstract

The geostationary constellation of meteorological satellites that is currently in operations opens interesting perspectives in the monitoring of surface properties that are characterized by a high variability in time. One of such properties is the Land Surface Temperature whose daily cycle may be retrieved thanks to the high frequency sampling that presently ranges from 15 min to 1 hour. Retrieval of LST from the geostationary constellation implies nevertheless solving for a number of difficulties that are linked to the radiometers on-board the different satellites, namely the range and number of available channels in the infrared window which constrain the algorithms to be used to retrieve LST.

Radiative transfer models are an indispensable tool when developing and assessing the quality of a given algorithm for LST retrieval. The so-called RTTOV (Radiative Transfer for TOVS) model is a fast radiative transfer model that is able to simulate radiances when given an atmospheric profile of temperature, variable gas concentrations, cloud and surface properties.

In the present work, we explore the potential of RTTOV both as a computationally-efficient means to invert the equation of radiative transfer in a channel centered about 10.8 μm and as a basis of development of a statistical mono-window procedure to retrieve LST. First the performance of RTTOV is evaluated for a very wide range of conditions. For this purpose a large number of synthetic values of brightness temperature are generated using a dataset of more than 10,000 atmospheric profiles, together with a wide variety of values of surface emissivity and viewing angles. Obtained top-of-atmosphere radiances are then related with LST using coefficients statistically obtained by means of linear regressions.

In order to estimate the error of LST retrievals assuming realistic uncertainties in the input data, an uncertainty component was added to surface emissivity as well as to temperature and humidity profiles using appropriate error covariance matrices. The top-of-atmosphere brightness temperatures were further perturbed according to the sensor expected noise.

Obtained results show that estimated LST presents RMSE (with respect to reference values) of 1.4K when using the physically-based approach based on RTTOV, and of 1.6K when using a statistically-based mono-window procedure.

Resumo

A constelação de satélites meteorológicos de órbita geostacionária, actualmente em funcionamento operacional, abre perspectivas interessantes para a monitorização de propriedades da superfície terrestre, nomeadamente as caracterizadas por elevada variabilidade temporal. De entre estas, destaca-se a temperatura da superfície do solo cujo ciclo diurno pode ser resolvido através de uma amostragem de alta frequência que, no caso da actual constelação de satélites geostacionários, varia no intervalo de 15 minutos até uma hora. No entanto, a determinação da temperatura à superfície a partir da constelação de satélites geostacionários implica ultrapassar algumas dificuldades relacionadas com as características dos diferentes radiómetros a bordo dos diferentes satélites, podendo mencionar-se, a título de exemplo, o número distinto de canais na janela do infravermelho e a diferente largura de banda dos próprios canais disponíveis, características essas que constituem constrangimentos ao tipo de algoritmo comum a utilizar para a determinação da temperatura da superfície do solo.

Os modelos de transferência radiativa constituem uma ferramenta indispensável quando se pretende desenvolver e testar a qualidade de um dado algoritmo de determinação da temperatura da superfície do solo. Neste particular, o modelo RTTOV é capaz de simular radiâncias no topo da atmosfera e perfis verticais da transmissividade da atmosfera, desde que se conheçam os respectivos perfis atmosféricos de temperatura e humidade, bem como as concentrações dos gases activos radiativamente que constituem a atmosfera seca e outras propriedades relativas às nuvens e à superfície do solo.

De forma a justificar a utilização do modelo RTTOV nesta dissertação, procede-se a uma avaliação sistemática do desempenho do RTTOV através do cálculo da radiância no topo da atmosfera e a da transmissividade da atmosfera, simuladas para uma vasta gama de perfis atmosféricos com o RTTOV, valores esses que são, em seguida, comparados com simulações, obtidas para condições idênticas, recorrendo ao modelo MODTRAN. Os resultados obtidos apontam para uma tendência para valores mais frios na temperatura de brilho simulada com o modelo RTTOV, relativamente ao modelo MODTRAN. Em termos de transmissividade, o modelo RTTOV apresenta, em geral, valores mais elevados que os do MODTRAN. Pode, assim, concluir-se que o RTTOV apresenta um comportamento mais "transparente" que o MODTRAN. O valor da raiz do erro quadrático médio (REQM) da transmissividade é de 0.04, que não difere em ordem de grandeza do valor do viés, de 0.03, sugerindo que a "transparência" do modelo RTTOV é sistemática e não aleatória. Uma REQM de 0.04 na transmissividade poderá ser relevante no caso de atmosferas secas, onde se podem atingir erros até 20%. Por outro lado, a REQM (viés) da temperatura de brilho no topo da atmosfera é de 0.21K (-0.04K), tendo-se neste caso que o erro é de cariz aleatório, e os erros máximos são da ordem de 0.1%. Estes resultados sugerem que o modelo RTTOV está de acordo com o modelo MODTRAN para a maioria dos casos, com excepção daqueles cuja atmosfera seja mais opaca, onde os erros na transmissividade podem ser relevantes. No entanto, o desempenho do modelo RTTOV é aceitável para aplicações em tempo quase real, especialmente tendo em conta o desempenho em termos de tempos de corrida, quando comparado com o MODTRAN.

No presente trabalho, explora-se o potencial do RTTOV como ferramenta computacionalmente eficiente para inverter a equação de transferência radiativa num canal centrado em 10.8 μm, e como

instrumento de base para o desenvolvimento de um mono-canal estatístico para determinar a temperatura da superfície do solo. Começa por proceder-se a uma avaliação do desempenho do RTTOV para uma gama vasta de condições atmosféricas e de superfícies do solo. Para tal, gera-se um elevado número de temperaturas de brilho sintéticas recorrendo a uma base de dados constituída por mais de 10 000 perfis atmosféricos, juntamente com uma ampla variedade de valores de emissividade à superfície e de ângulos de visão do satélite. Em seguida, relaciona-se as radiâncias obtidas (no topo da atmosfera) com as respectivas temperaturas à superfície, utilizando coeficientes obtidos estatisticamente através de regressões lineares.

A fim de estimar o erro na determinação da temperatura da superfície do solo, assumem-se incertezas nos dados de entrada, nomeadamente uma componente de incerteza associada ao ruído do radiómetro a bordo do satélite, uma outra componente associada à emissividade da superfície do solo e uma terceira associada aos perfis de temperatura e humidade, sendo, neste último caso, a incerteza estimada a partir das matrizes de covariância dos erros do modelo operacional do Centro de Previsão do Tempo a Prazo Médio.

Os resultados obtidos mostram que a temperatura da superfície do solo estimada apresenta uma raiz do erro quadrático médio de 1.4K quando se utiliza o método físico baseado no RTTOV, valor este que aumenta em cerca de 15%, para 1.6K, quando se recorre ao método estatístico, baseado em regressões lineares. Quando subdivididos em classes de vapor de água na atmosfera e na emissividade do solo, o método físico apresenta sempre um desempenho ligeiramente superior, com excepção do caso de atmosferas húmidas conjugadas com elevada emissividade da superfície do solo, onde o desempenho do método estatístico apresenta um valor mais baixo da raiz do erro quadrático médio.

Se bem que, em termos globais, o método físico apresente um desempenho superior ao método estatístico, a simplicidade deste último método aliada ao facto de o primeiro requerer um conhecimento preciso de termos da equação de transferência radiativa que são, normalmente, difíceis de estimar por serem sensíveis às incertezas no perfil da atmosfera abre perspectivas interessantes para a utilização, de forma operacional e em tempo quase real, do método estatístico para determinar a temperatura da superfície do solo com base em informação fornecida por uma constelação de satélites geostacionarios.

Neste contexto se antevê que o método estatístico desenvolvido na presente dissertação venha a constituir a base para o desenvolvimento de um novo produto operacional de determinação da temperatura da superfície do solo baseado nos satélites GOES e MTSAT a desenvolver no contexto do “Copernicus Global Land Service”.

List of Figures

List of Tables

List of Acronyms

AVHRR	Advanced Very High Resolution Radiometer
CMDL	Climate Monitoring & Diagnostics Laboratory
ECMWF	European Centre for Medium-range Weather Forecast
EUMETSAT	EUropean organization for the exploitation of METeorological SATellites
ESA	European Space Agency
GOES	Geostationary Operational Environmental Satellite
GSW	Generalized Split-Windows
LSE	Land Surface Emissivity
LST	Land Surface Temperature
LWIR	Long-Wave InfraRed
MODTRAN	MODerate resolution atmospheric TRANsmission
MSG	Meteosat Second Generation
MTSAT	Multi-Functional Transport Satellite
MW	Mono-Window
NOAA	National Oceanic and Atmospheric Administration
NWP	Numerical Weather Prediction
PMW	Physical Mono-Window
RMSE	Root Mean Squared Error
RTE	Radiative Transfer Equation
RTM	Radiative Transfer Model
RTTOV	Radiative Transfer for TOVS
SAF	Satellite Application Facility
SEVIRI	Spinning Enhanced Visible and InfraRed Imager
SMW	Statistical Mono-Window
SZA	Satellite Zenith Angle
TCWV	Total Column Water Vapor
TIGR-3	Thermodynamic Initial Guess Retrieval
TIR	Thermic InfraRed
TIROS	Television Infrared Observation Satellite
TOA	Top-Of-Atmosphere
TOVS	TIROS Operational Vertical Sounder
TTM	Two Temperature Method

TABLE OF CONTENTS

CHAPTER 1

1.1 THESIS GOAL

Land Surface Temperature is a key parameter in the physics of land surface processes since it is involved in the surface energy budget. LST is the primary variable determining the upward thermal radiation and one of the main controllers of sensible and latent heat fluxes between the surface and the atmosphere. Therefore, a reliable estimation of LST is of great importance for a wide number of applications, which include model validation [1], data assimilation [2], hydrological applications [3] and climate monitoring [4]–[5].

The geostationary constellation of meteorological satellites that is currently in operations opens interesting perspectives in the monitoring of surface properties that are characterized by a high variability in time. LST is one of these properties whose daily cycle may be retrieved thanks to the high frequency sampling that presently ranges from 15 min to 1 hour. Retrieval of LST from the geostationary constellation implies nevertheless solving for a number of difficulties that are linked to the own characteristics of the radiometers on-board the different satellites, namely the range and number of available channels in the infrared window which constrain the algorithms to be used to retrieve LST.

Radiative transfer models are an indispensable tool when developing and assessing the quality of a given algorithm for LST retrieval. The so-called RTTOV[1] model is a fast radiative transfer model that is able to simulate radiances when given an atmospheric profile of temperature, variable gas concentrations, cloud and surface properties [6].

The goal of this dissertation is to explore the potential of the RTTOV model both as a computationally efficient means to invert the equation of radiative transfer in an infrared channel centered about 10.8 μm and as a basis of development of a statistical mono-window procedure to retrieve LST.

1.2 THESIS ORGANIZATION

The second chapter gives a general overview on radiometric quantities; the essential laws that rule blackbody radiation; and the radiative transfer equation in the infrared window of the electromagnetic spectrum. Two radiative transfer models, RTTOV and MODTRAN, are described in the third chapter and values of brightness temperature, radiances and transmissivity as obtained from the forward run of the two models are compared, using in both models the same dataset consisting of thousands of atmospheric profiles with a wide variety of values of surface emissivity, surface temperatures and viewing angles.

[1] RTTOV is an acronym that contains an acronym that contains another acronym: RTTOV means Radiative Transfer for TOVS, where TOVS means TIROS Operational Vertical Sounder and TIROS means in turn Television Infrared Observation Satellite.

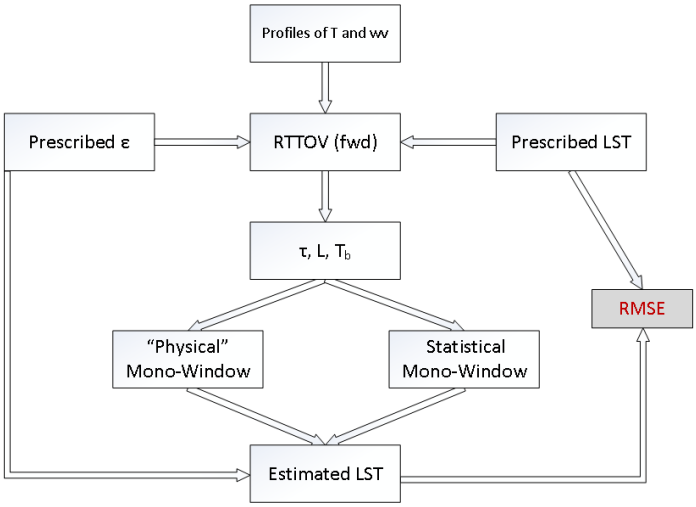

Figure 1.1 – Organization chart summarizing the methodology applied in Chapter 3. In the above scheme, T is the temperature profile, wv is the water vapor profile, ε is the surface emissivity, τ is the atmospheric transmittance, L is the TOA radiance and T_b the brightness temperature.

In the fourth chapter, the simulated values of top-of-atmosphere brightness temperature, transmissivity and radiances are used to invert the equation of radiative transfer and obtain estimated LSTs. Two methods are discussed: (1) a "physical" approach which consists in the simple inversion of RTTOV, and (2) a statistical approach where top-of-atmosphere radiances are related with LST by means of a linear model whose coefficients are statistically obtained by least squares regressions. In order to estimate the error of LST retrievals assuming realistic uncertainties in the input data, an uncertainty component is added to surface emissivity as well as to temperature and humidity profiles using appropriate error covariance matrices. The top-of-atmosphere brightness temperatures are also perturbed according to the sensor expected noise. Figure 1.1 schematically shows the procedure that is followed in this chapter.

CHAPTER 2

"It cannot be seen, cannot be felt,
Cannot be heard, cannot be smelt,
It lies behind stars and under hills,
And empty holes it fills,
It comes first and follows after,
Ends life, kills laughter."

J.R.R. Tolkien in *The Hobbit* – 1937

2.1 THEORETICAL BACKGROUND

This dissertation builds upon some theoretical concepts that are worth being mentioned. In the present chapter a succinct view on the laws of radiation is provided and the radiative transfer equation (*RTE)* is introduced.

2.1.1 Basic Radiometric Quantities

Radiance L, and irradiance E are two important quantities in radiation theory. Let us consider a differential amount of monochromatic radiant energy, dQ_ν, defined in a given time interval dt and in a specific frequency domain $[\nu, \nu + d\nu]$, within an element of volume dV, travelling in a given direction confined to a differential solid angle $d\Omega$. This amount dQ_ν will be given by

$$dQ_\nu = h\nu f_\nu(\vec{r}, \vec{\Omega}, t) dV dt d\Omega d\nu \tag{2.1}$$

where f_ν is the so-called distribution function of photons, which depends on position $\vec{r}$, solid angle $\vec{\Omega}$ and time t, and where $h\nu$ is the energy of one photon (h being the Planck's constant). Considering that the radiation crosses an element of area dS, and that α is the angle between the direction of propagation of radiation and the normal to the surface, then during the time interval dt the surface will be crossed by the photons contained in the volume element $dV = dScdtcos(\alpha)$; one therefore obtains from equation (2.1) :

$$d\Phi_\nu = \frac{dQ_\nu}{dt} = h\nu f_\nu(\vec{r}, \vec{\Omega}, t) dScd\Omega d\nu \cos(\alpha) \tag{2.2}$$

where $d\Phi_\nu$ is the monochromatic radiant power, also referred to as monochromatic radiant flux.

Spectral radiance L_ν is the fundamental quantity in radiation theory, being defined as the monochromatic flux per unit projected area per unit solid angle, i.e.:

$$L_\nu = \frac{d\Phi_\nu}{dScos(\alpha)d\Omega d\nu} \tag{2.3}$$

The SI units of radiance are $[W/m^2/sr/s^{-1}]$ but in remote sensing applications it is customary to use traditional units, such as $[mW/m^2/sr/cm^{-1}]$. From (2.2) and (2.3) it may be concluded that $L_\nu = h\nu f_\nu(\vec{r}, \vec{\Omega}, t)$.

Monochromatic irradiance E_ν is defined as the rate at which the monochromatic radiant flux is delivered to a surface, i.e.:

$$E_\nu = \frac{d\Phi_\nu}{dSd\nu} \tag{2.4}$$

From equation (2.3) it may be concluded that:

$$E_\nu = \int_\Omega L_\nu cos(\alpha) d\Omega \tag{2.5}$$

i.e. monochromatic irradiance is given by the normal component of L_ν integrated over the entire hemispheric solid angle. In the case of Lambertian surfaces, i.e., when radiance is the same in all directions we have,

$$E_\nu = \pi L_\nu \tag{2.6}$$

Figure 2.1 represents a beam of radiance L_ν impinging on a given body. Part of the total incident radiance may be reflected backwards, part may be absorbed due to the molecular properties of the body and the radiance exiting the body may be attenuated throughout its path inside the body. Based on the fractions of total radiance that are reflected L_r, absorbed L_a or transmitted L_t , one may accordingly define reflectivity r, absorptivity α, and transmittance τ:

$$r = \frac{L_r}{L} \tag{2.7}$$

$$\alpha = \frac{L_a}{L} \tag{2.8}$$

$$\tau = \frac{L_t}{L} \tag{2.9}$$

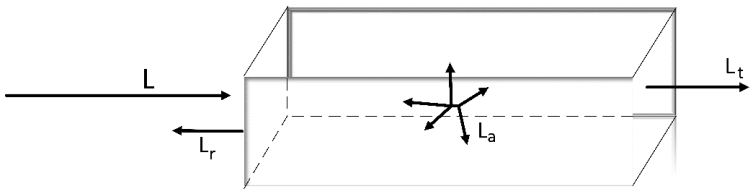

Figure 2.1 – A beam of radiance L is impinging on a body and fractions of that radiance are reflected, absorbed and transmitted.

Since conservation of energy implies that:

$$L = L_a + L_r + L_t \tag{2.10}$$

then dividing by the total radiance it yields that

$$\frac{1}{L}L = \frac{1}{L}(L_a + L_r + L_t) = \alpha + r + \tau = 1 \tag{2.11}$$

2.1.2 The Thermal Infrared window

Figure 2.2 illustrates the atmospheric transmission spectra showing the windows available for Earth observations in the infrared domain [7].

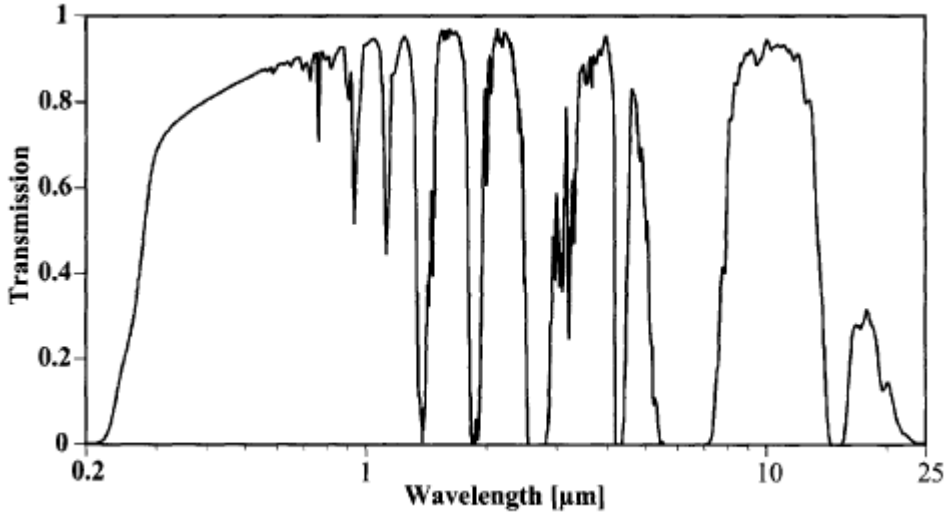

Figure 2.2 – Atmospheric transmission spectra showing windows available for Earth observations [7].

The Long-Wave InfraRed (LWIR), sometimes called Thermal InfraRed (TIR) is defined in the range from 8 to 15 µm [8]. At this wavelength interval, energy radiated by the earth's surface and clouds is not significantly attenuated by atmospheric gases. In this channel, most surfaces and cloud types have high values of emissivity close to 1, a notable exception being thin cirrus. Therefore, the brightness temperature sensed by the satellite is close to the actual surface skin or cloud top temperature for scenes other than cirrus. Usually instruments on-board satellites have channels centered around 10.8 and 12 µm channels. Channel 12 µm, sometimes referred to as the "dirty" channel, has the property of absorbing increased amounts of radiation due to low-level moisture (http://rammb.cira.colostate.edu).

2.1.3 Blackbody Radiation

A blackbody is an ideal surface or cavity that has the property that all incident electromagnetic radiation flux is completely absorbed, i.e., has zero reflectivity and transmissivity, and absorptivity equal to one [7].

2.1.3.1 Planck's law

The amount and quality of the energy emitted by a blackbody are uniquely determined by its temperature, as given by Planck's law [9], which in the wavelength domain is written as,

$$B(T,\lambda) = \frac{2hc^2}{\lambda^5(e^{hc/\lambda K_B T} - 1)} \tag{2.12}$$

where B is the spectral radiance of the blackbody, K_B is the Boltzmann constant, c is the speed of light, and T is the absolute temperature. It is worth noting that Planck's function, $B(T,\lambda)$ is not a point function, it is a distribution, and for that reason from now on it will be referred to as Planck's distribution. Therefore, when converting Planck's distribution from wavelength domain to frequency domain the total radiance computed within a given interval $[\lambda_1, \lambda_2]$ has to be preserved when computed over the corresponding interval $[\nu_1, \nu_2]$ [10]. From the definition of spectral radiance, radiance $B(T)$ emitted by a blackbody with temperature T is given by:

$$B(T) = \int_{\lambda_1}^{\lambda_2} B(\lambda,T)d\lambda \quad \Leftrightarrow \quad dB(T) = B(\lambda,T)d\lambda \tag{2.13a,b}$$

Differentiating equation $\nu\lambda = c$ in order to frequency,

$$\frac{d\lambda}{d\nu} = -\frac{c}{\nu^2} \tag{2.14}$$

and substituting in equation (2.13a), one obtains:

$$\int_{\lambda_1}^{\lambda_2} B(\lambda,T)d\lambda = \int_{\nu_1}^{\nu_2} B(\nu,T)\frac{d\lambda}{d\nu}d\nu = \int_{\nu_1}^{\nu_2} -B(\nu,T)\frac{c}{\nu^2}d\nu$$

When $\lambda_1 > \lambda_2$ one has $\nu_1 < \nu_2$ and it is therefore natural to rewrite the previous relationship as follows:

$$\int_{\lambda_1}^{\lambda_2} B(\lambda,T)d\lambda = \int_{\nu_2}^{\nu_1} B(\nu,T)\frac{c}{\nu^2}d\nu \tag{2.15}$$

Substituting in equation (2.12) and rearranging, one obtains Planck distribution in frequency:

$$B(\nu, T) = \frac{2h\nu^3}{c^2\left(e^{h\nu/K_BT} - 1\right)} \tag{2.16}$$

2.1.3.2 Kirchhoff's law

The Kirchhoff's law of thermal radiation says that, for any given body, its emissivity equals absorptivity. Since emissivity is a physical property, this statement may be proven by considering an isolated system consisting of two bodies in thermal equilibrium, one being a blackbody and the other a non-blackbody.

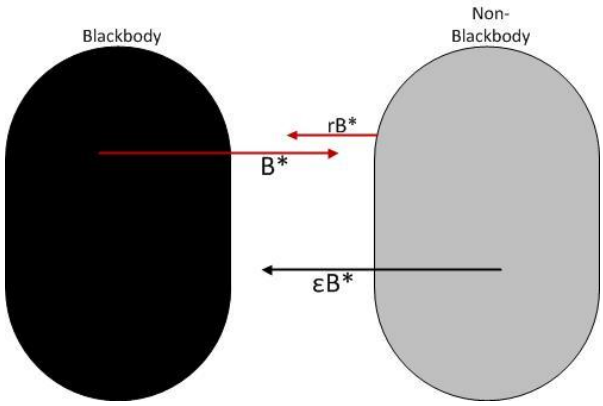

Figure 2.3 – Balance of energy between a blackbody (black filled) and a non-blackbody (grey filled) in thermal equilibrium.

The blackbody emits a quantity B^* and the non-blackbody a fraction ε of B^*, as shown in Figure 2.3. Since the blackbody does not reflect any energy, the reflection term is only from the non-blackbody. The equilibrium may accordingly be written as

$$B^* = \varepsilon B^* + rB^* \tag{2.17}$$

and simplifying,

$$1 = \varepsilon + r \tag{2.18}$$

Since the system is isolated, the transmittance is null and therefore one has from equation (2.11) that the reflectivity is $r = 1 - \alpha$. Equation (2.18) becomes therefore,

$$1 = \varepsilon + (1 - \alpha) \tag{2.19}$$

which may be simplified to the Kirchhoff's law of radiation:

$$\varepsilon = \alpha \tag{2.20}$$

2.1.4 The Radiative Transfer Equation

Figure 2.4 provides a schematic overview of the contributions to the total infrared radiation as measured by a sensor at the top of the atmosphere. The energy path that carries information about the temperature of a given object is the one going from the target object towards the sensor (*L1* in Figure 2.4). This radiance will be a function of Planck's distribution modified by the wavelength-dependent emissivity of the target [7]. This radiance will be also attenuated by the transmittance along the target sensor path, and is written as,

$$L^{TOA}(\lambda,\theta) = \varepsilon(\lambda,\theta)B(T,\lambda)\tau_s(\lambda,\theta) \tag{2.21}$$

where $\varepsilon(\lambda,\theta)$ is the wavelength and viewing angle, θ, dependent emissivity, $B(T,\lambda)$ is the spectral radiance for a blackbody at temperature T as described by Planck distribution, (2.12), and $\tau_s(\lambda,\theta)$ is the surface to space wavelength and viewing angle dependent transmittance.

According to Kirchhoff's law, an opaque object with emissivity ε will have reflectivity $r = 1 - \varepsilon$. So, another important contribution to the infrared radiative transfer equation is the radiance reflected by the surface from the surroundings due to its temperature. As the Earth's surface is not a blackbody, the downward radiance emitted by the atmosphere may be reflected by it and propagated upwards to the sensor (L2 in Figure 2.4). This term is combined with (2.21) and yields,

$$L^{TOA}(\lambda,\theta) = \varepsilon(\lambda,\theta)B(T,\lambda)\tau_s(\lambda,\theta) + \big(1-\varepsilon(\lambda,\theta)\big)L_d\tau_s(\lambda,\theta) \tag{2.22}$$

where L_d is the downward radiance emitted by the atmosphere.

Equation (2.22) lacks a contribution due to self-emitted radiance from the atmosphere along the line of sight [7]. This upwelled radiance term (L3 in Figure 2.4) can be expressed as upward radiance emitted by each atmospheric layer, as

$$L_{up} = \int_{\tau_s}^{1} B(\lambda,T)d\tau \tag{2.23}$$

where the atmospheric layers begin at the ground level, τ_s, and end with the layer just below the sensor. So the full infrared radiative transfer equation is obtained by adding term (2.23) to (2.22),

$$\begin{aligned} L^{TOA}(\lambda,\theta) = \varepsilon(\lambda,\theta)B(T,\lambda)\tau_s(\lambda,\theta) + \int_{\tau_s}^{1} B(\lambda,T)d\tau \\ + \big(1-\varepsilon(\lambda,\theta)\big)L_d\tau_s(\lambda,\theta) \end{aligned} \tag{2.24}$$

This equation represents the radiance that upwells from Earth's surface and atmosphere and reaches the sensor, in the infrared portion of the electromagnetic spectrum.

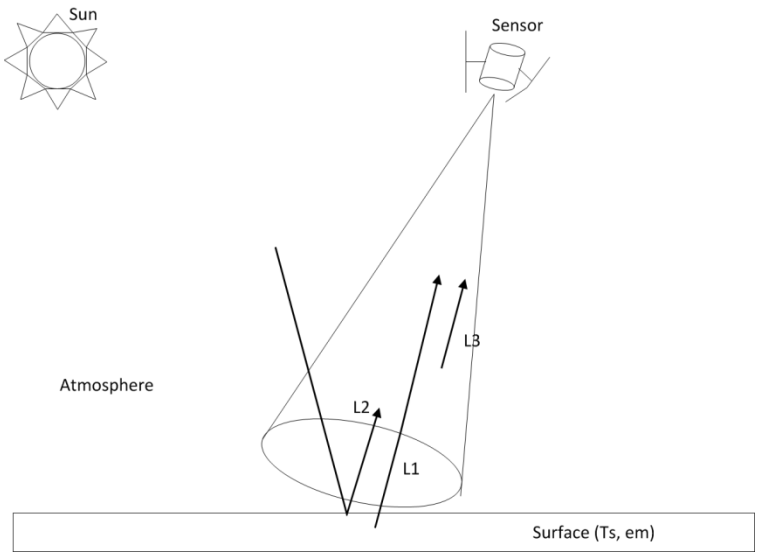

Figure 2.4 – Relationship between terms in the radiative transfer equation (2.24) and energy paths associated with the photon flux onto the sensor.

CHAPTER 3

"Proposition IX: Radiant light consists in Undulations of the Luminiferous Aether."

Thomas Young in "Philosophical transactions" – 1802

3.1 INTRODUCTION

When Thomas Young introduced Proposition IX he was far from knowing the evolution that science would see in the two following centuries. He was far from dreaming that Einstein would introduce the relativity theory about one hundred years later, without recurring to the luminiferous aether he so devotedly defended. Thomas Young, a man of notable contributions to the fields of vision, light, solid mechanics, energy, physiology, language, musical harmony and even Egyptology [11], was far from thinking about computers and even farther from dreaming about radiative transfer models that allow simulating thousands of atmospheric profiles, and with a simple "click" getting the respective thousands of top-of-atmosphere radiances. As Thomas Young, scientists of nowadays cannot know what is coming in the next couple of centuries, but they can help improving what we already know by giving little baby steps or giant steps. In the last decades the radiative transfer model (RTM) LOWTRAN/MODTRAN has been the standard model in the scientific community, however it's not a very fast model. A new and faster RTM has been developed in the last few years, the RTTOV, with the purpose of being used in the assimilation cycles of Numerical Weather Prediction (NWP) models. The RTTOV is a semi-empirical model that is capable of computing the various terms of the radiative transfer equation for a wide range of built-in bands and viewing geometries of passive infrared and microwave satellite radiometers, spectrometers and interferometers [6]. RTTOV is validated, by comparison with simulations performed by state-of-the-art line-by-line or band models, such as MODTRAN. This chapter provides an introduction to RTMs and, in order to justify its use in Chapter 4, the RTTOV model is validated against MODTRAN.

3.2 RADIATIVE TRANSFER MODELS

3.2.1 The RTTOV model

RTTOV is a fast radiative transfer model for TOVS, originally developed at ECMWF in the beginning of the 90's. Subsequently the original model has undergone several developments, more recently within the EUMETSAT NWP Satellite Application Facility (SAF, http://research.metoffice.gov.uk/research/interproj/nwpsaf/). This thesis relies on version 10 of RTTOV which is the latest version. The model allows fast simulations of radiances for satellite infrared or microwave nadir scanning radiometers given an atmospheric profile of temperature, variable gas concentrations, cloud and surface properties, referred as the state vector. The only mandatory variable gas is water vapor, which will be the only variable gas profile used here. However other gases like ozone, carbon dioxide, nitrous oxide, methane and carbon monoxide may be used as variables in the state vector. RTTOV accepts input profiles on any defined set of

pressure levels. The spectral range of the RTTOV model in the infrared is $3-20\ \mu m$ ($500-3000\ cm^{-1}$) [6].

The platform that will be simulated in this work with RTTOV is the METEOSAT Second Generation, MSG, i.e., the geostationary meteorological satellites developed by the European Space Agency, ESA, in close cooperation with the European Organization for the Exploitation of Meteorological Satellites, EUMETSAT. The MSG playload includes the Spinning Enhanced Visible and Infrared Imager (SEVIRI), which provides high temporal resolution images (15min) together with a spatial resolution (3km at subsatellite point) appropriate to regional to continental scales. In addition, SEVIRI presents spectral capabilities that are very similar to the TIR bands around 10.8 and 12.0 μm of the Advanced Very High Resolution Radiometer (AVHRR) on-board the National Oceanic and Atmospheric Administration (NOAA) series.

RTTOV uses one form of equation (2.24), where the reflected downwelled radiance is written in its integral form,

$$L^{TOA}(\lambda,\theta) = \varepsilon(\lambda,\theta)B(T_s,\lambda)\tau_s(\lambda,\theta) + \int_{\tau_s}^{1} B(\lambda,T)d\tau + \big(1-\varepsilon(\lambda,\theta)\big)\tau_s^2(\lambda,\theta)\int_{\tau_s}^{1}\frac{B(\lambda,T)}{\tau^2(\lambda,\theta)}d\tau \tag{3.1}$$

and where transmittances, τ, are computed by means of a linear regression in the optical depth based on variables from the input profile vector [6].

3.2.2 The MODTRAN model

The MODerate spectral resolution atmospheric TRANsmittance algorithm (MODTRAN4) is a "narrow band model" atmospheric radiative transfer code. The atmosphere is modeled as a stratified (horizontally homogeneous) medium, and its constituent profiles, both molecular and particulate, may be defined either using built-in models or by user-specified vertical profiles. The spectral range extends from the UV into the far-infrared, providing resolution as fine as $0.2\ cm^{-1}$. MODTRAN solves the radiative transfer equation taking into consideration the effects of molecular and particulate absorption/emission and scattering, surface reflections and emission, solar/lunar illumination, and spherical refraction [12].

MODTRAN outputs include narrow spectral band direct and diffuse transmittances, path component and total radiances, transmitted and top-of-atmosphere solar/lunar irradiances, and horizontal fluxes [12].

3.2.3 Output Variables

Let us consider a simplified version of RTE (2.24) and (3.1),

$$L^{TOA}(\lambda,\theta) = \varepsilon(\lambda,\theta)B(T_s,\lambda)\tau_s(\lambda,\theta) + L_{up} + \big(1-\varepsilon(\lambda,\theta)\big)\tau_s(\lambda,\theta)L_{down} \tag{3.2}$$

where the integrals are represented by L_{up} and L_{down} for the atmospheric upwelling and downwelling, respectively. When a radiative transfer model is run in the forward scheme, the main outputs are the top-of-atmosphere radiance and/or the respective brightness temperature and the surface-to-space transmissivity. Validation of results from RTTOV will be performed by comparing the outputs for these three terms with the respecting ones as obtained from MODTRAN.

3.3 DATABASE OF ATMOSPHERIC PROFILES

The simulations are performed using database of global profiles [13] of temperature and water vapor for clear sky conditions. This training database includes global profiles taken from NOAA-88 , ECMWF training sets, TIGR-3, ozonesondes from 8 NOAA Climate Monitoring and Diagnostics Laboratory sites, CMDL, and radiosondes from 2004 in the Sahara desert. Skin temperature over land surfaces corresponds to LST in the dataset and is estimated as a function of 2-m temperature and solar zenith and azimuth angles. From the total of 15 700 profiles, a subset of 4712 was selected that coincide with the MSG/SEVIRI disk. Figure 3.1 plots the geographical positions of the chosen profiles.

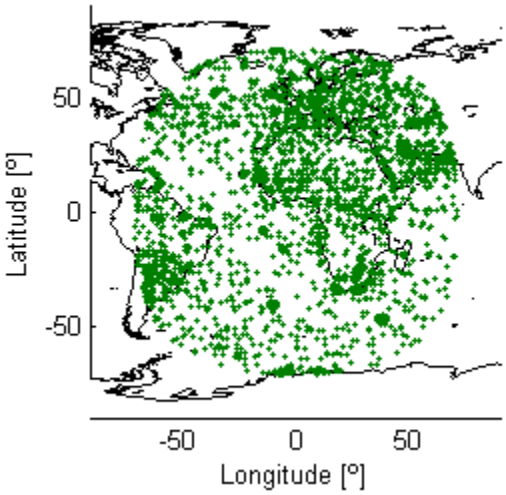

Figure 3.1 – Geographical location of the chosen subset of profiles.

Figure 3.2 shows the histograms of LST, total column water vapor (TCWV), emissivity and viewing angle. The great majority of emissivity values lie in the 0.94 – 0.99 interval and more than 40% of them are within the 0.99 bin. Viewing angle presents a biased distribution since there is a shortage of profiles with angles between 0 and 40° when compared with the number of profiles at higher angles. TCWV also has a biased distribution that favors dryer atmospheres.

In order to constrain the retrieval errors, profiles with SZA higher than 50º and clear sky atmospheric profiles with TCWV greater than 6cm were not considered. The dataset was accordingly further reduced to about 2000 profiles.

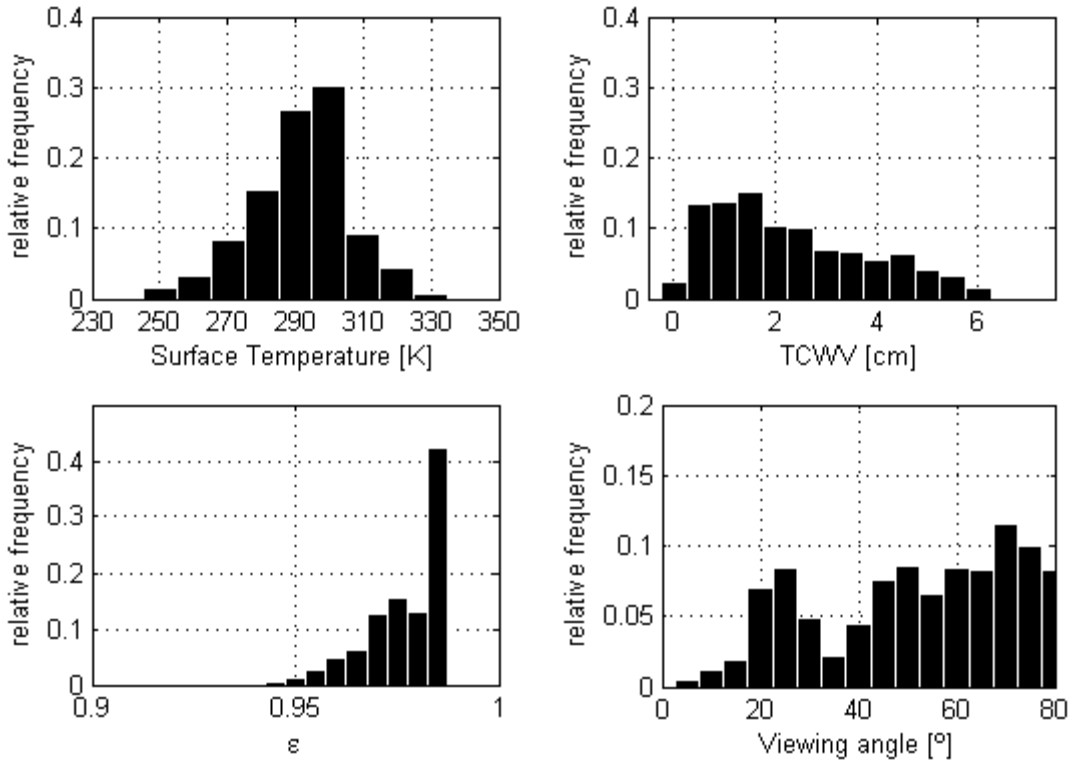

Figure 3.2 – Histograms of surface temperature (top left), total column water vapor (top right), emissivity (bottom left) and viewing angle (bottom right) respecting to the used dataset.

3.4 VALIDATION OF RTTOV

Figure 3.3 shows the distributions of the three considered variables (i.e. brightness temperature, top-of-atmosphere radiance and transmittance) for RTTOV and MODTRAN. The distribution of brightness temperature presents a peak around $293\ K$, indicating a good agreement between the models, with the RMSE (bias) being 0.21 K (-0.04 K). TOA radiance distributions are once again in agreement, presenting a RMSE (bias) of 0.34 $mW/m^2/sr/cm^{-1}$ (0.11 $mW/m^2/sr/cm^{-1}$) and a peak around $100\ mW/m^2/sr/cm^{-1}$.

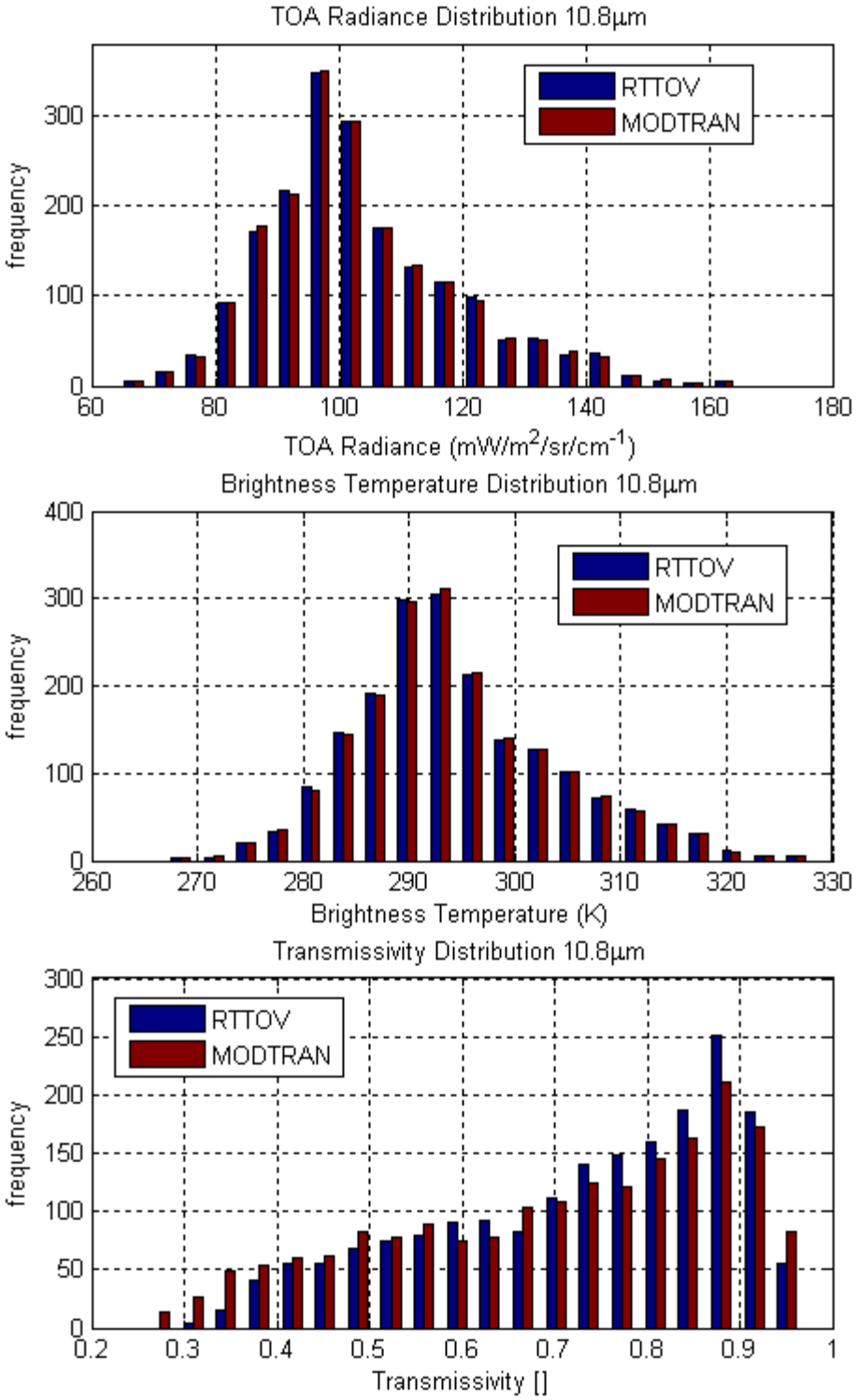

Figure 3.3 – Histograms of brightness temperature (top), TOA radiance (middle) and transmittance (bottom) for RTTOV (blue) and MODTRAN (red).

The distribution of transmittance is the one presenting the higher differences between the two models. The histogram shows that for small values of transmittance there is a small fraction of RTTOV data, when compared with MODTRAN, namely for values smaller than 0.4. On the other hand, for values greater than 0.7 the frequency of RTTOV's transmittance is greater than MODTRAN. As a result, the range of transmittance values generated with RTTOV tends to be narrower than that of MODTRAN simulations. Transmittance RMSE (bias) is 0.04 (0.03).

An analysis was also performed on the statistical distribution of differences between simulated values of brightness temperature and of transmittance, as simulated by RTTOV and by MODTRAN. If brightness temperature and transmittance are generally denoted by X, then differences between simulations are computes as

$$\Delta X = X_{RTTOV} - X_{MODTRAN} \tag{3.3}$$

As schematically shown in Figure 3.4, the statistical distributions of ΔX are estimated by scanning the space of TCWV vs. SZA by a matrix of 2 cm in TCWV by 20º in SZA in steps of 1 cm by 1º. As shown in Figure 3.5, for each position of the scanning matrix, values of medium and of median of ΔX, as well as of values of differences between these two estimates are computed and plotted in TCWV vs. SZA space using the respective centroid of the matrix for location.

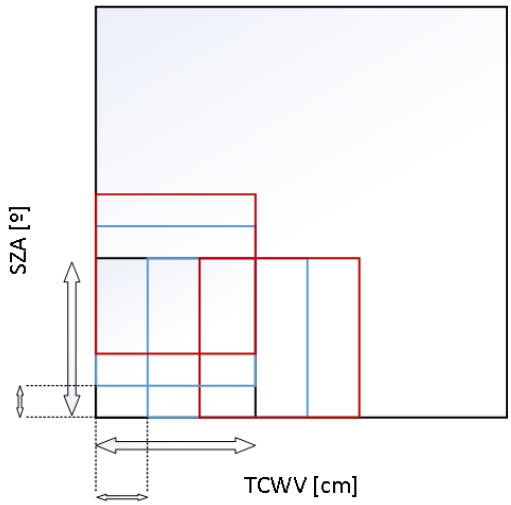

Figure 3.4 – A schematic representation of the method used to characterize the statistical distribution of differences between estimates from RTTOV and MODTRAN.

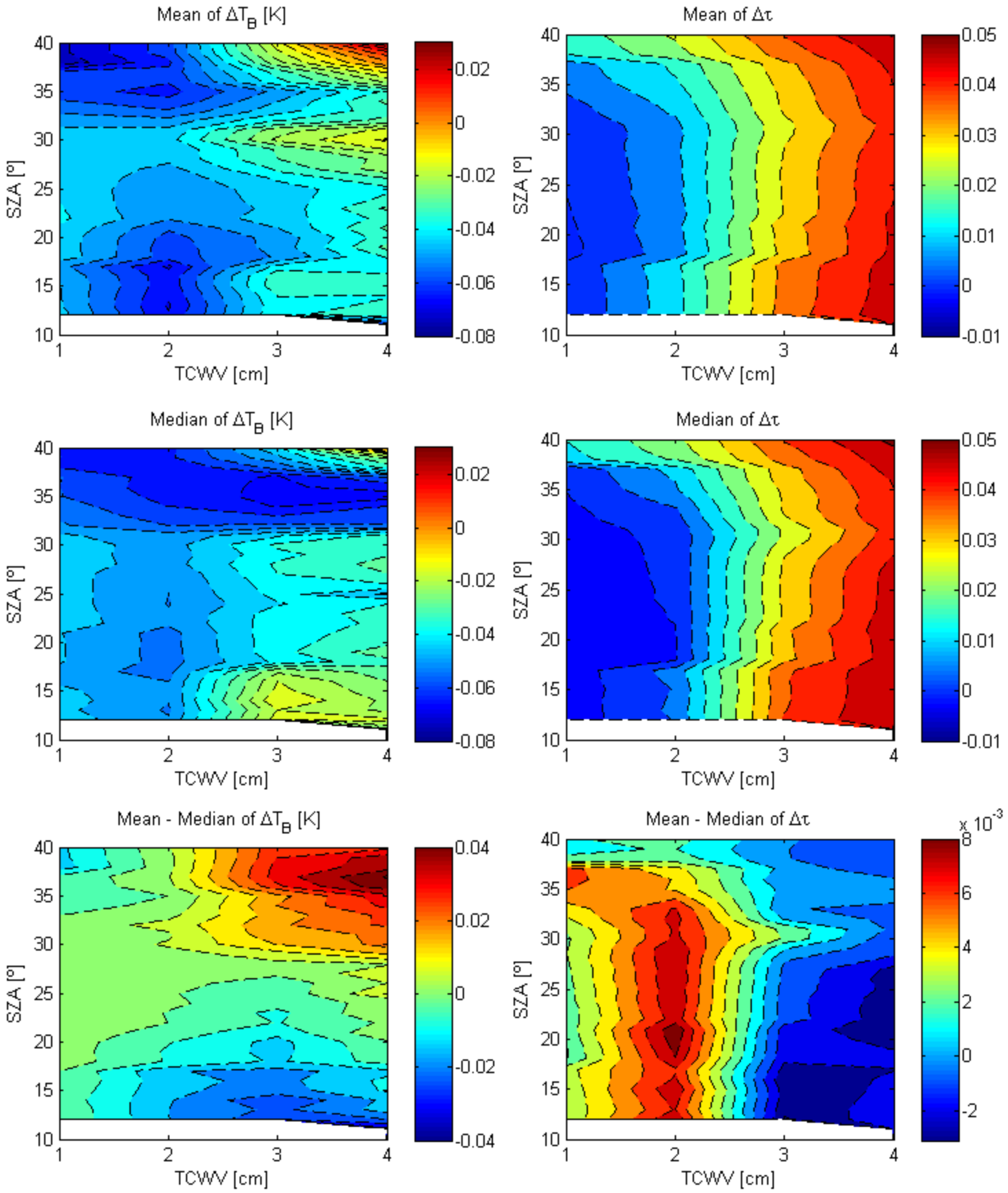

Figure 3.5 – Mean (top), median (middle) and mean minus median (bottom) of the differences between RTTOV and MODTRAN brightness temperatures (left) and transmittances (right).

As shown in Figure 3.5 (left panels), the RTTOV estimates of brightness temperature tend to be slightly cooler (0.02 to 0.08K) than those from MODTRAN. RTTOV estimates of transmittance (right panels) are generally higher than by MODTRAN, a result that is in agreement with obtained differences in brightness temperature. However, transmittance discrepancies present a clearer dependence on TCWV, both mean and median differences increasing with water vapor content.

In the case of the difference between the means and the medians of brightness temperature (Figure 3.5, lower left panel), results suggest that (1) the RTTOV brightness temperature tends to be consistently higher than MODTRAN for high SZA as TCWV evolves from dry to moist atmospheres; and (2) MODTRAN brightness temperature tend to be higher than RTTOV for low SZA as TCWV goes from lower to higher values.

Differences of departures of means of transmittance from respective medians (Figure 3.5, lower right panel) show in turn positive values for drier atmospheres and negative values for the moister ones, an indication that estimates of transmittance by RTTOV tend to be higher (lower) than those by MODTRAN for drier (moister) atmospheres. These results support the abovementioned conclusion that RTTOV behaves as a more "transparent" model when compared to MODTRAN.

CHAPTER 4

“”Science studies everything,” say the scientists. But, really, everything is too much. Everything is an infinite quantity of objects; it is impossible at one and the same time to study all. As a lantern cannot light up everything, but only lights up the place on which it is turned or the direction in which the man carrying it is walking, so also science cannot study everything, but inevitably only studies that to which its attention is directed. And as a lantern lights up most strongly the place nearest to it, and less and less strongly objects that are more and more remote from it, and does not at all light up those things its light does not reach, so also human science, of whatever kind, has always studied and still studies most carefully what seems most important to the investigators, less carefully what seems to them less important, and quite neglects the whole remaining infinite quantity of objects. ... But men of science to-day ... have formed for themselves a theory of “science for science's sake,” according to which science is to study not what mankind needs, but everything.”

Lev Tolstoi in “Modern Science”, Essays and Letters – 1903

4.1 INTRODUCTION

A controversial way of characterizing scientists and the science that is born from them, some may say. But after all, what does mankind needs? It is a difficult question that will probably never be answered. Nevertheless “everything” is a good start. “Science studies everything”, says the common mortal[2]. “But, really, everything is too much”, replies the scientist[3]. If the scientist is going for a walk, the common mortal comes and asks if it will rain on its birthday, far, far away from now. The scientist pulls out his pencil and starts to solve an impossible equation. After a few minutes of impossible solutions the scientist says: “it may or may not rain”. Outraged by the scientist’s response the common mortal decides to blame science, scientists and everything that reminded him of that “poor men answer”, for not knowing what to wear on its birthday. After all, the scientist works without rest, even if he has to solve impossible things, just to satisfy the common mortal, and the common mortal blames science and the scientist for its inaccuracy in understanding and answering EVERYTHING he wants.

The common mortal decides to continue throwing questions to the scientist, this time wanting to know if there is a quick way to decide where is the best place to grow a farm of lettuce and carrots, based on knowledge of the perfect temperature of the soil to accomplish that, and having a simple geostationary satellite with an infrared sensor, which only has top-of-atmosphere radiance as output and only works with one spectral window. The poor scientist grabs the pencil once again and starts to write…

[2] Common mortal as the arithmetic mean of all mankind: a general personification.
[3] The scientist here is not seen as better, worse or different, but just a particular case of the common mortal.

4.2 THE INVERSION PROBLEM

Equation (3.1) represents the direct (or forward) problem, where the atmospheric state is known (namely temperature and humidity profiles), and the LST and LSE are prescribed and used as inputs to the RTM (which in the particular case of this dissertation will be RTTOV). Based on the RTM forward run, simulated radiances are estimated, together with estimates of the respective brightness temperature and surface-to-space transmittances (see Chapter 3). In turn, the inverse problem consists in using the simulated (or observed) top-of-atmosphere radiances and, knowing the atmospheric profiles and LSE, estimate the LST. This simple inversion, using only one spectral window, will be here referred to as the Mono-Window MW algorithm ([14]–[16]). Other algorithms, with different approaches, like the split-windows [17]–[19] or TTM methods [20] are currently being used by the scientific community. A simple and practical way to determine whether or not a given model is mathematically invertible consists in executing three simple steps: (1) select a set of values for land surface temperature (LST) and land surface emissivity (LSE) and the respective atmospheric profiles; (2) use the forward model to compute values of top-of-atmosphere radiance associated with each of those surface variables and atmospheric profiles; and (3) using the computed values as perfect observations (i.e. error free measurements), evaluate the surface parameters through the inversion of equation (3.1) [21].

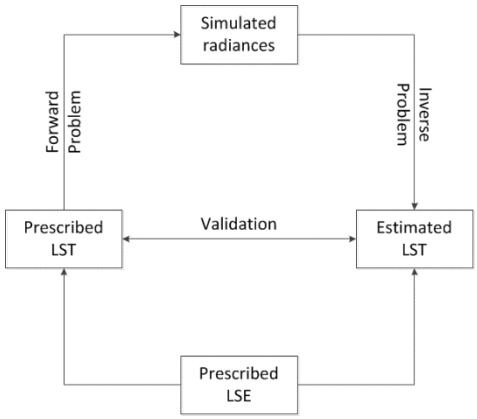

Figure 4.1 – Schematic representation of the problem of LST estimation and of the method used to test the sensitivity of the mono-window algorithm (Based on [20]).

The model is considered as invertible if the estimated value of LST is close enough to the prescribed one. If the process is repeated for a large set of surface and atmospheric conditions, then the robustness of the results tends to increase. This procedure may be further generalized by perturbing the observations [20]. Figure 4.1 presents a scheme of the problem of LST estimation from observed radiance, using a mono-window algorithm.

4.3 "PHYSICAL" MONO-WINDOW

The so called "physical" mono-window (PMW) is a pseudo-physic algorithm, since it is the simple inversion of RTTOV, which is not a purely physical model but a pseudo-empirical one. The term "physical" is here used to contrast with the statistical mono-window that will be introduced in the next section.

When inverting the simplified version of the radiative transfer equation, (3.2), the result is the following,

$$B(T_S,\lambda) = \frac{L^{TOA}(\lambda,\theta) - L_{up} - \big(1-\varepsilon(\lambda,\theta)\big)\tau_s(\lambda,\theta)L_{down}}{\varepsilon(\lambda,\theta)\tau_s(\lambda,\theta)} \tag{4.1}$$

The calibrated Planck function in the frequency domain for a channel of finite width (see equation (2.16)) may be approximated as [22],

$$B(T_S,\nu) \approx \frac{c_1\nu_c^3}{\exp\left(\frac{c_2\nu_c}{[\alpha T_s+\beta]}\right)-1} \tag{4.2}$$

where c_1, c_2, are constants and α, β and ν_c depend on the spectral characteristics of the channel to be used. Surface temperature is then computed by inverting equation (4.2),

$$T_s \approx \frac{c_2\nu_c\alpha^{-1}}{\log\left(\frac{c_1\nu_c^3}{B}+1\right)} - \beta \tag{4.3}$$

The main problem in inverting radiative transfer equation (4.1) is that emissivity is multiplying transmittance in the denominator. Since both terms are within the interval $[0,1]$ and transmittances can be as small as 0.3, the result of equation (4.1) is very sensitive to small errors in transmittance and emissivity, which would then be propagated as large errors in LST retrievals. This problem may be mitigated by using the bisection method. The process may be understood by considering the merging of equations (4.1) and (4.2),

$$\underbrace{\frac{c_1\nu_c^3}{\exp\left(\frac{c_2\nu_c}{[\alpha T_s+\beta]}\right)-1}}_{\boldsymbol{A}} \approx \underbrace{\frac{L^{TOA}(\lambda,\theta) - L_{up} - \big(1-\varepsilon(\lambda,\theta)\big)\tau_s(\lambda,\theta)L_{down}}{\varepsilon(\lambda,\theta)\tau_s(\lambda,\theta)}}_{\boldsymbol{B}} \tag{4.4}$$

Since emissivity and transmittance are in the denominator of term B it is convenient to move them to term A in order to avoid any numerical problems with the division as mentioned above,

$$\underbrace{\varepsilon(\lambda,\theta)\tau_s(\lambda,\theta)\frac{c_1\nu_c^3}{\exp\left(\frac{c_2\nu_c}{[\alpha T_m+\beta]}\right)-1}}_{\boldsymbol{C_m}} \approx \underbrace{L^{TOA}(\lambda,\theta) - L_{up} - \big(1-\varepsilon(\lambda,\theta)\big)\tau_s(\lambda,\theta)L_{down}}_{\boldsymbol{C}} \tag{4.5}$$

Since LST is almost always greater than brightness temperature one may take as starting temperatures the brightness temperature itself and the brightness temperature with an increment of 20K, as exemplified in Figure 4.2. The first step of the bisection method is to divide the total interval in two equal parts, by simply finding the mean value , T_m, of the left and right temperatures. Then T_m is used to compute term C_m. If this new value of C_m is greater than term C

then it means that actual LST is lower than T_m. In the second iteration the temperature "to the right" changes to previous T_m , whereas the temperature "to the left" is kept unchanged and the same procedure is repeated. The iterations stop when the difference between temperatures "to the right" and "to the left" is less than 0.01 K.

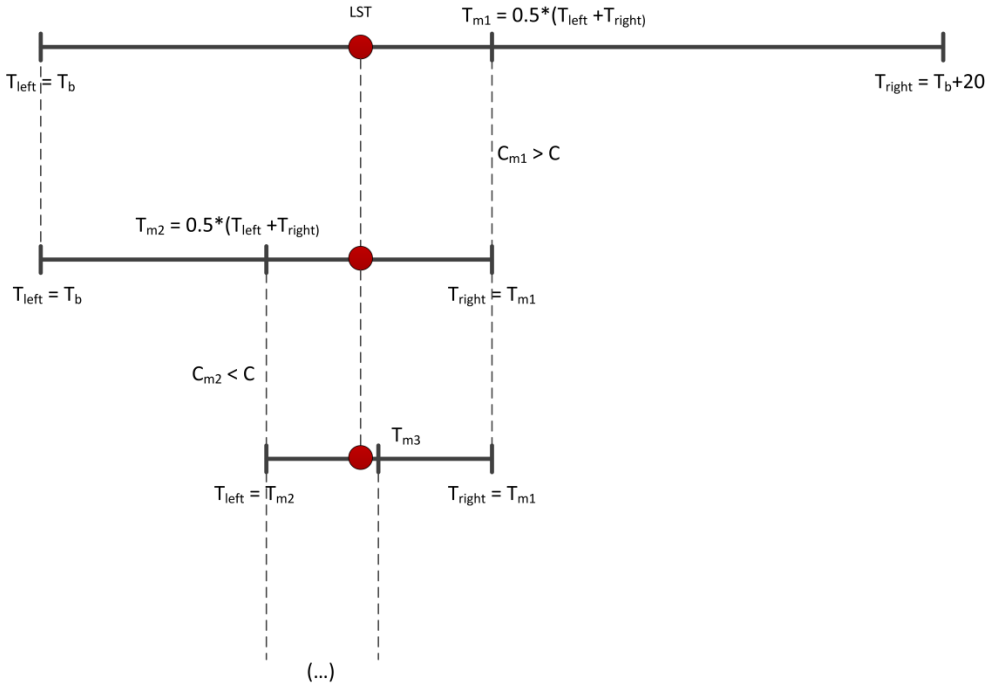

Figure 4.2 – Schematic representation of the bisection algorithm.

4.4 STATISTICAL MONO-WINDOW

The statistical mono-window (SMW) algorithm differs from the "physical" mono-window (PMW) in two main aspects: (1) it does not depend explicitly on the atmospheric profiles of temperature and humidity and; (2) it does not need intermediate terms of equation (3.1). This algorithm lies on the linear relationship between surface temperature and brightness temperature, as shown in Figure 4.3. If coefficients of that linear relationship are estimated by least squares, then once the brightness temperature at the top of the atmosphere is known, surface temperature may be computed in a straightforward manner. However this algorithm can be improved if the regression coefficients depend on viewing angle, total column water vapor and emissivity.

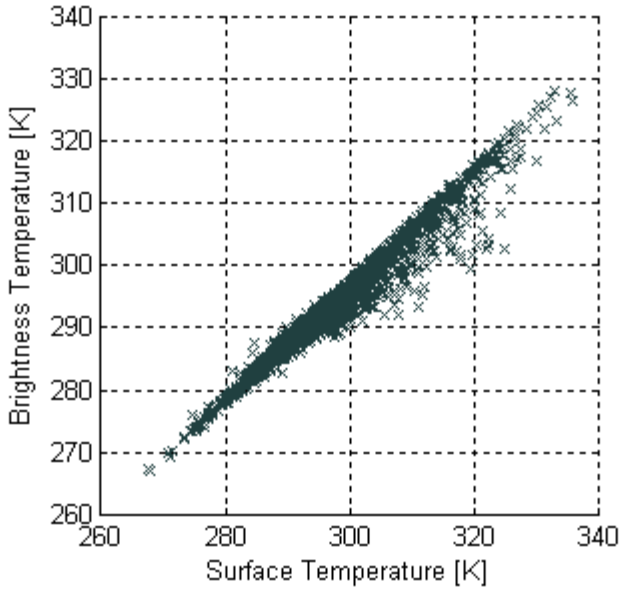

Figure 4.3 – Relation between surface temperature (prescribed) and RTTOV computed brightness temperature.

Considering equation (3.2), and replacing $L^{TOA}(\lambda,\theta)$ by the Planck distribution in terms of brightness temperature, one has:

$$B(T_b,\lambda) = \varepsilon(\lambda,\theta)B(T_s,\lambda)\tau_s(\lambda,\theta) + L_{up} + \big(1-\varepsilon(\lambda,\theta)\big)\tau_s(\lambda,\theta)L_{down} \qquad (4.7)$$

Considering equation (2.23), and applying the mean-value theorem:

$$L_{up} = \int_{\tau_s}^{1} B(\lambda,T)d\tau = B(\lambda,\bar{T}_a)\int_{\tau_s}^{1} d\tau \qquad (4.8)$$

where $\bar{T}_a$ is a mean temperature of the atmospheric column.

Solving the integral one obtains:

$$L_{up} = \big(1-\tau_s(\lambda,\theta)\big)B(\lambda,\bar{T}_a) \qquad (4.9)$$

In case of the downwelling term, by a similar reasoning one obtains from equation (3.1) and (3.2):

$$\tau_s(\lambda,\theta)L_{down} = \tau_s^2(\lambda,\theta)\int_{\tau_s}^{1}\frac{B(\lambda,T)}{\tau^2}d\tau \qquad (4.10)$$

Considering again a mean atmospheric temperature and applying the mean-value theorem to the integral in τ, it yields,

$$\tau_s(\lambda,\theta)L_{down} = \tau_s(\lambda,\theta)\big(1-\tau(\lambda,\theta)\big)B(\lambda,\bar{T}_a) \tag{4.11}$$

Using a Taylor series to expand Planck's distribution around some temperature T_* near T_b, T_s and $\bar{T}_a$ one has:

$$B(\lambda,T_s) \approx B(\lambda,T_*) + \frac{\partial B(\lambda,T_*)}{\partial T}(T_s - T_*) \tag{4.12}$$

$$B(\lambda,T_b) \approx B(\lambda,T_*) + \frac{\partial B(\lambda,T_*)}{\partial T}(T_b - T_*) \tag{4.13}$$

and

$$B(\lambda,\bar{T}_a) \approx B(\lambda,T_*) + \frac{\partial B(\lambda,T_*)}{\partial T}(\bar{T}_a - T_*) \tag{4.14}$$

Applying equations (4.9) and (4.11) to equation (4.7) and rearranging terms, one is led to:

$$\begin{aligned} B(T_b,\lambda) = {} & \varepsilon(\lambda,\theta)B(T_s,\lambda)\tau_s(\lambda,\theta) \\ & + [1-\tau(\lambda,\theta)]\big[1+\big(1-\varepsilon(\lambda,\theta)\big)\tau(\lambda,\theta)\big]B(\lambda,\bar{T}_a) \end{aligned} \tag{4.15}$$

Substituting equations (4.12), (4.13) and (4.14) in (4.15) and organizing the terms dependent of $B(\lambda,T_*)$ it yields,

$$\begin{aligned} & B(\lambda,T_*) + \frac{\partial B(\lambda,T_*)}{\partial T}(T_b - T_*) \\ & \quad = \big\{\varepsilon(\lambda,\theta)\tau(\lambda,\theta) \\ & \quad + [1-\tau(\lambda,\theta)]\big[1+\big(1-\varepsilon(\lambda,\theta)\big)\tau(\lambda,\theta)\big]\big\}B(\lambda,T_*) \\ & \quad + \varepsilon(\lambda,\theta)\tau(\lambda,\theta)\frac{\partial B(\lambda,T_*)}{\partial T}(T_s - T_*) \\ & \quad + [1-\tau(\lambda,\theta)]\big[1+\big(1-\varepsilon(\lambda,\theta)\big)\tau(\lambda,\theta)\big]\frac{\partial B(\lambda,T_*)}{\partial T}(\bar{T}_a \\ & \quad - T_*) \end{aligned} \tag{4.16}$$

Considering that the term dependent on τ^2 may be neglected, then:

$$\varepsilon(\lambda,\theta)\tau(\lambda,\theta) + [1-\tau(\lambda,\theta)]\big[1+\big(1-\varepsilon(\lambda,\theta)\big)\tau(\lambda,\theta)\big]$$
$$= \varepsilon(\lambda,\theta)\tau(\lambda,\theta) + \big(1-\tau(\lambda,\theta)\big)$$
$$+ \big(1-\tau(\lambda,\theta)\big)\tau(\lambda,\theta)\big(1-\varepsilon(\lambda,\theta)\big) \tag{4.17}$$
$$= \varepsilon(\lambda,\theta)\tau(\lambda,\theta) + \big(1-\tau(\lambda,\theta)\big) + \tau(\lambda,\theta)$$
$$- \varepsilon(\lambda,\theta)\tau(\lambda,\theta) = 1$$

and equation (4.16) becomes,

$$\frac{\partial B(\lambda,T_*)}{\partial T}(T_b - T_*)$$
$$= \varepsilon(\lambda,\theta)\tau(\lambda,\theta)\frac{\partial B(\lambda,T_*)}{\partial T}(T_s - T_*)$$
$$+ [1-\tau(\lambda,\theta)]\big[1+\big(1-\varepsilon(\lambda,\theta)\big)\tau(\lambda,\theta)\big]\frac{\partial B(\lambda,T_*)}{\partial T}(\bar{T}_a \tag{4.18}$$
$$- T_*)$$

Eliminating the derivatives,

$$0 = \varepsilon(\lambda,\theta)\tau(\lambda,\theta)(T_s - T_*) + [1-\tau(\lambda,\theta)]\big[1+\big(1-\varepsilon(\lambda,\theta)\big)\tau(\lambda,\theta)\big](\bar{T}_a \tag{4.19}$$
$$- T_*)$$

then solving for T_s and rearranging the terms dependent on T_b , the ones dependent on $\bar{T}_a$, and the ones dependent on T_*, one has:

$$T_s$$
$$= \frac{1}{\varepsilon(\lambda,\theta)\tau(\lambda,\theta)}T_b - \left[\frac{\big(1-\varepsilon(\lambda,\theta)\big)}{\varepsilon(\lambda,\theta)} + \frac{\big(1-\tau(\lambda,\theta)\big)}{\varepsilon(\lambda,\theta)\tau(\lambda,\theta)}\right]\bar{T}_a \tag{4.20}$$
$$+ \underbrace{\left[1 + \frac{\big(1-\varepsilon(\lambda,\theta)\big)}{\varepsilon(\lambda,\theta)} + \frac{\big(1-\tau(\lambda,\theta)\big)}{\varepsilon(\lambda,\theta)\tau(\lambda,\theta)} - \frac{1}{\varepsilon(\lambda,\theta)\tau(\lambda,\theta)}\right]}_{=\mathbf{0}} T_*$$

It is easily verified that the third term on the right handside of equation (4.20) is zero, and thus,

$$T_s = \frac{1}{\varepsilon(\lambda,\theta)\tau(\lambda,\theta)}T_b - \left[\frac{\big(1-\varepsilon(\lambda,\theta)\big)}{\varepsilon(\lambda,\theta)} + \frac{\big(1-\tau(\lambda,\theta)\big)}{\varepsilon(\lambda,\theta)\tau(\lambda,\theta)}\right]\bar{T}_a \tag{4.21}$$

Considering all the terms in equation (4.21),

$$T_s = \frac{1}{\varepsilon(\lambda,\theta)\tau(\lambda,\theta)} T_b - \frac{\big(1-\varepsilon(\lambda,\theta)\big)}{\varepsilon(\lambda,\theta)} \bar{T}_a - \frac{\big(1-\tau(\lambda,\theta)\big)}{\varepsilon(\lambda,\theta)\tau(\lambda,\theta)} \bar{T}_a \tag{4.22}$$

and simplifying,

$$T_s = \frac{1}{\varepsilon(\lambda,\theta)\tau(\lambda,\theta)} T_b - \frac{\bar{T}_a}{\varepsilon(\lambda,\theta)} + \bar{T}_a - \frac{1}{\varepsilon(\lambda,\theta)\tau(\lambda,\theta)} \bar{T}_a + \frac{\bar{T}_a}{\varepsilon(\lambda,\theta)} \tag{4.23}$$

the equation may be rewritten as,

$$T_s = \frac{1}{\varepsilon(\lambda,\theta)\tau(\lambda,\theta)} T_b - \frac{\bar{T}_a}{\varepsilon(\lambda,\theta)\tau(\lambda,\theta)} + \bar{T}_a \tag{4.24}$$

Since transmittance is only a function of TCWV and viewing angle and $\bar{T}_a$ only depends on TCWV, the two terms may be replaced by coefficients $a = 1/\tau(\lambda,\theta)$, $b = \bar{T}_a/\varepsilon(\lambda,\theta)$ and $c = \bar{T}_a$,

$$T_s = a\frac{T_b}{\varepsilon(\lambda,\theta)} + b\frac{1}{\varepsilon(\lambda,\theta)} + c \tag{4.25}$$

Coefficients a, b and c may be estimated by linear regression. Figure 4.4 shows these coefficients and Figure 4.5 shows the error variance of the fitted regression and the coefficient of determination. These coefficients were estimated with the near 2000 simulations of top-of-atmosphere brightness temperatures as computed when the selected profiles from the database were fed into RTTOV. The runs were executed by considering that each profile could be seen by the satellite for SZA from 0° to 50° with steps of 1°, meaning that the regression coefficients were estimated using more than 100 000 simulations.

The coefficients vary smoothly and almost vertically except for coefficient c. For classes of very moist atmospheres with high viewing angles the error variance of surface temperature by top-of-atmosphere brightness temperature tends to be considerably high (over 10%). The root mean squared error of LST estimated with the SMW, with the so-called perfect observations of brightness temperature, emissivity and atmospheric profiles, against the prescribed surface temperature is 1.22K. On the other hand, when the same procedure is applied with PMW, the RMSE is of 0.11K.

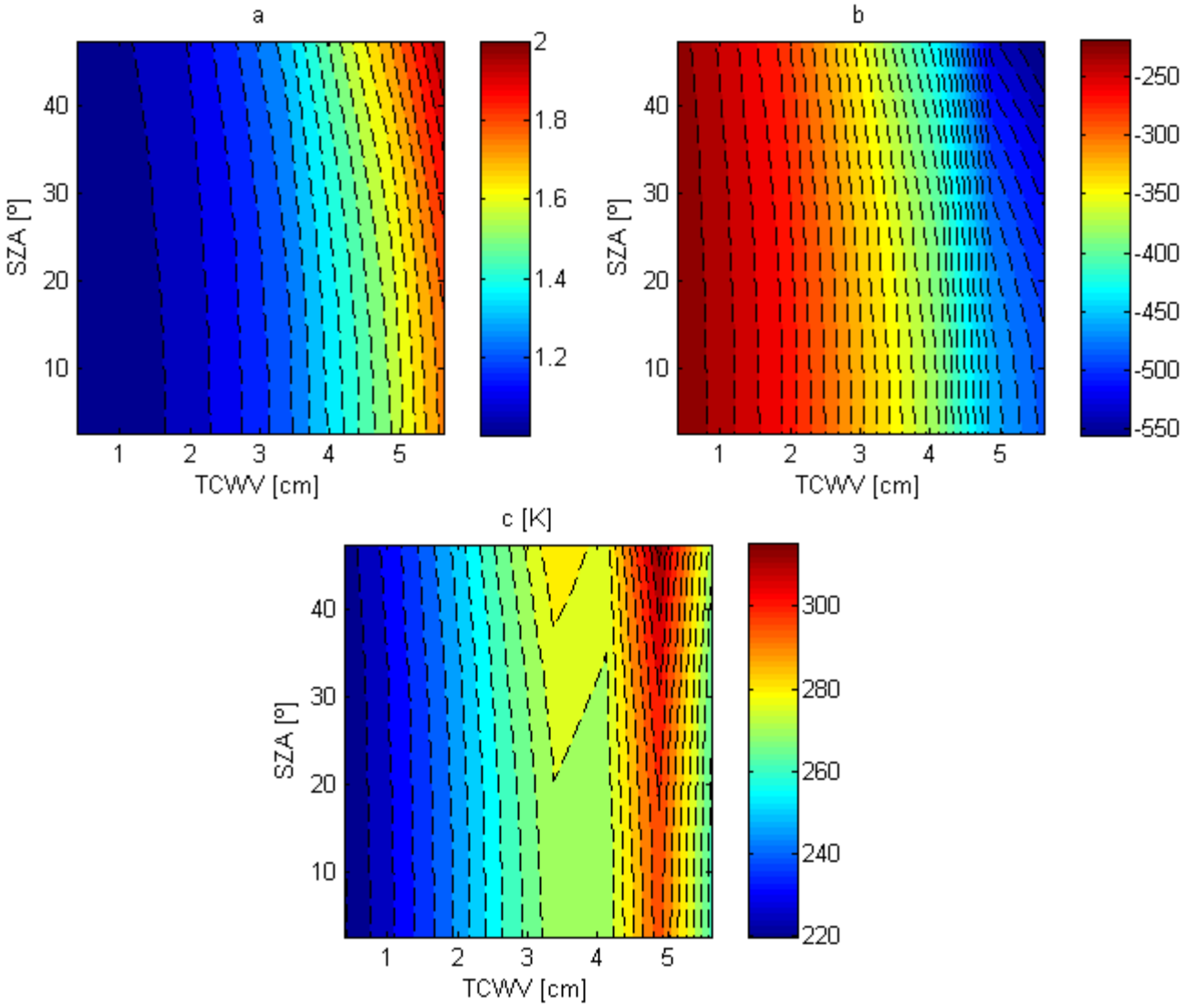

Figure 4.4 – Distribution of the SMW parameters (indicated at the top of each panel) as a function of the SZA and total column water vapor (in centimeters).

4.5 Error Propagation

In a real scenario, the mono-window inputs, $[T_b, \varepsilon]$ as well as the temperature and humidity profiles, are not known in their exact form. Therefore, LST as computed with the "physical" and statistical mono-window should include new sources of errors. The impact of these sources on LST uncertainties is the subject of the present section. Potentially, all inputs may induce errors in the retrieved LST values. However, here, only the radiometric noise, the uncertainty in surface emissivity and errors in the profiles of temperature and humidity, are considered [23].

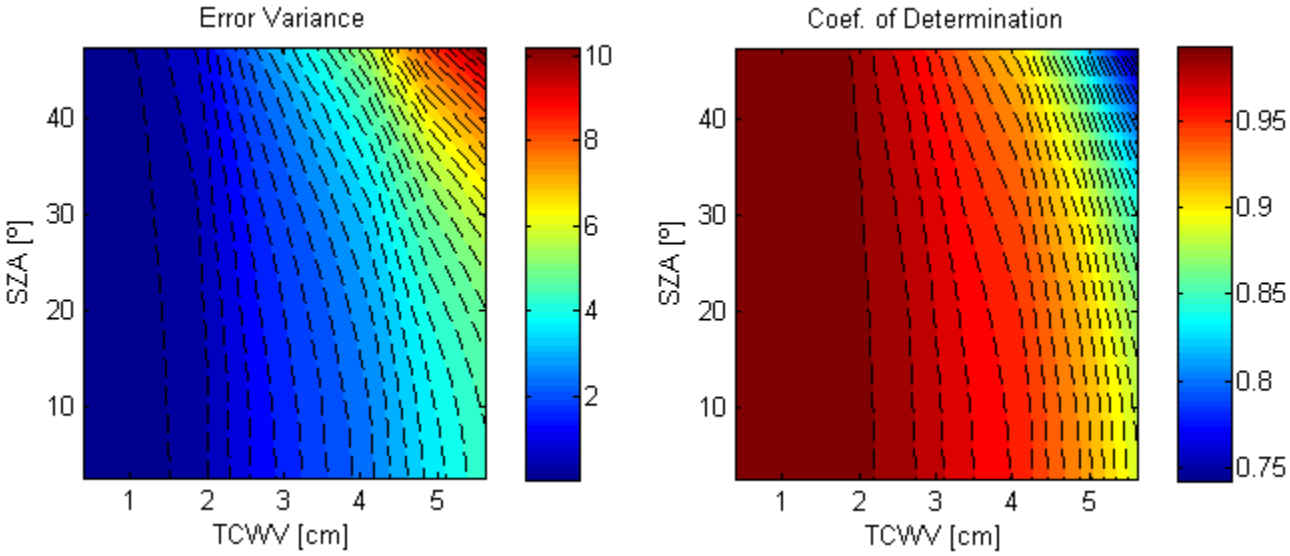

Figure 4.5 – Distribution of the error variance of the fitted regression and the coefficient of determination as a function of SZA and total column water vapor (in centimeters).

These sources are applied both to PMW and SMW algorithms. However SMW is affected by fewer perturbations than PMW as shown in Table 4.1.

Table 4.1 – List of PMW and SMW variables which propagate the error.

		PMW	**SMW**
Instrument Noise		√	√
Emissivity		√	√
Atmospheric Profiles	T	√	X
	WV	√	√

4.5.1 Instrument Noise

Performance of PMW and SMW is first assessed by taking into consideration the sensivity of the algorithms to noise in SEVIRI channel 10.8 μm. The used value for the noise is based on radiometric performances defined as short-term errors that include random noise, stability of temperature of detectors, crosstalk and straylight, stability of gain and electromagnetic perturbation [20]. Generated values for the brightness temperature noise were generated from a uniform random distribution within the interval $[-0.3, 0.3]$ K. Top-of-atmosphere radiance was then computed with these randomly perturbed values of brightness temperature.

4.5.2 Emissivity

The performance of the mono-window algorithms is then evaluated by taking in consideration errors in the prescribed emissivity. Errors in emissivity were generated from a random uniform distribution within the interval $[-0.02, 0.02]$.

4.5.3 Atmospheric Profiles

There are several ways of introducing errors in the temperature and humidity profiles. These atmospheric parameters may be perturbed with some fixed error percentage (e.g. $\pm$ 2%). However it is worth noting that this type of perturbation is not realistic because atmospheric profile errors do not induce similar changes on the atmospheric parameters. An alternative approach might consist in perturbing each level with values randomly taken from a normal distribution of zero mean and a standard deviation characteristic of the uncertainty. In this case, perturbations at a given level are assumed to be independent from those at other levels but such a procedure is also not realistic [20]. In the case of this dissertation a more realistic approach was adopted. For each profile, 10 new sets of perturbed profiles of temperature and humidity were generated based on the background error covariance matrix of the currently operational 4D-Var data assimilation scheme at ECMWF.

A covariance matrix is a matrix whose element in position i, j is the covariance between the i^{th} and j^{th} elements of a vector of random variables. Each element of the vector is a scalar random variable, either with a finite number of observed empirical values or with a finite or infinite number of potential values specified by a theoretical joint probability distribution of all the random variables [24]. In order to get the perturbed profiles, a Cholesky decomposition is used, i.e. a decomposition of a Hermitian, positive-definite matrix $\boldsymbol{M}$ into the product of a lower triangular matrix and its conjugate transpose,

$$\boldsymbol{M} = \boldsymbol{L}\boldsymbol{L}^{*} \tag{4.26}$$

where $\boldsymbol{L}$ is a lower triangular matrix with positive diagonal entries, and $\boldsymbol{L}^{*}$ is its conjugate transpose. Figure 4.6 shows examples of perturbed profiles of temperature and humidity (comparable with [20]). When using this purely mathematical procedure, some of the perturbed humidity profiles may have levels with negative values due to the proximity to zero of the reference profile. This problem may be circumvented by simply setting to zero the negative values.

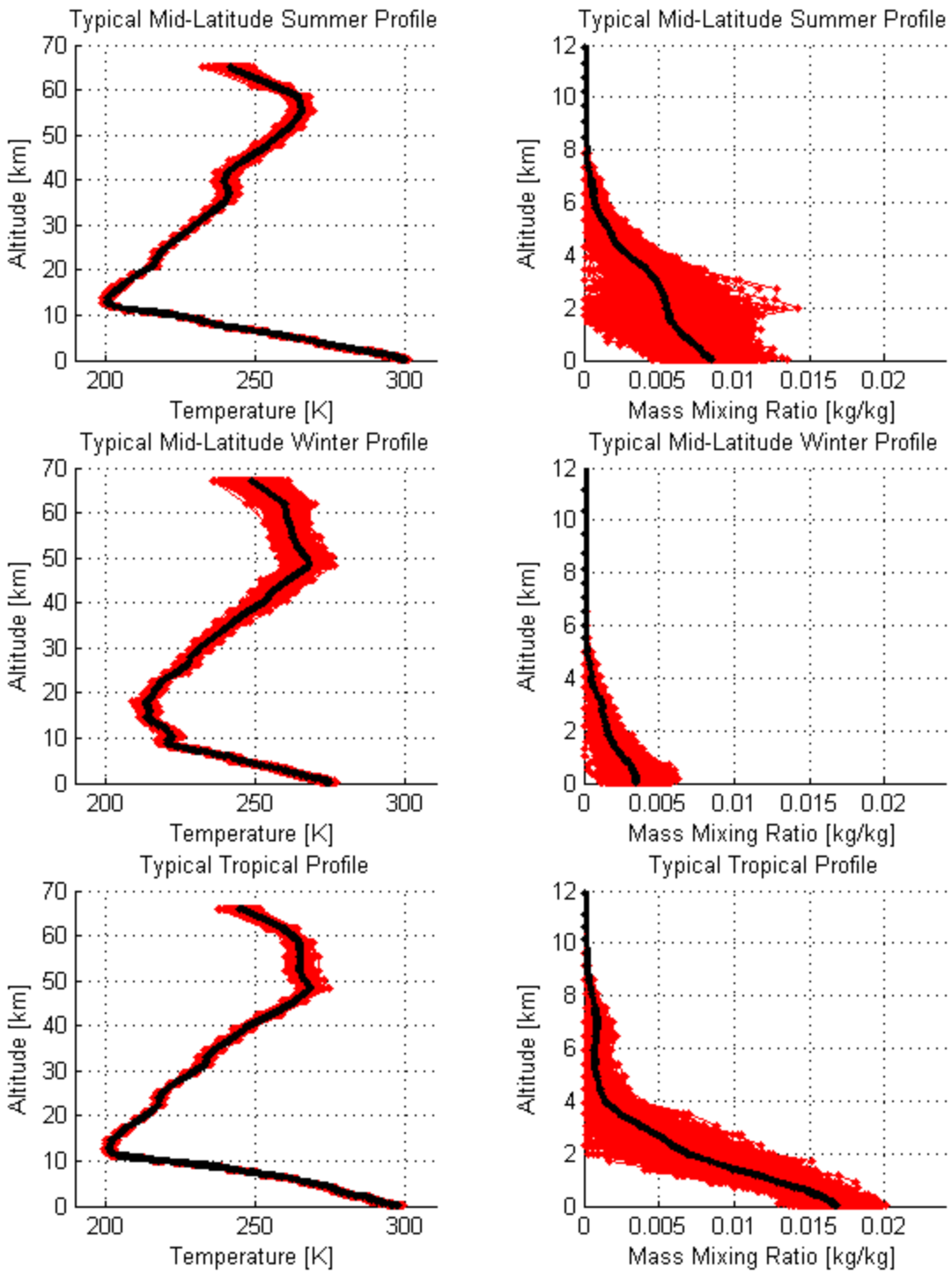

Figure 4.6 – Examples of typical Mid-Latitude Summer (top), Mid-Latitude Winter (middle) and Tropical (bottom) profiles of temperature and humidity – the thick black line – in comparison with 1000 perturbed profiles of temperature and humidity generated with the covariance matrixes – the red lines.

Figure 4.7 shows the histogram of the differences between prescribed TCWV and perturbed one for the same profiles as in Figure 4.6.

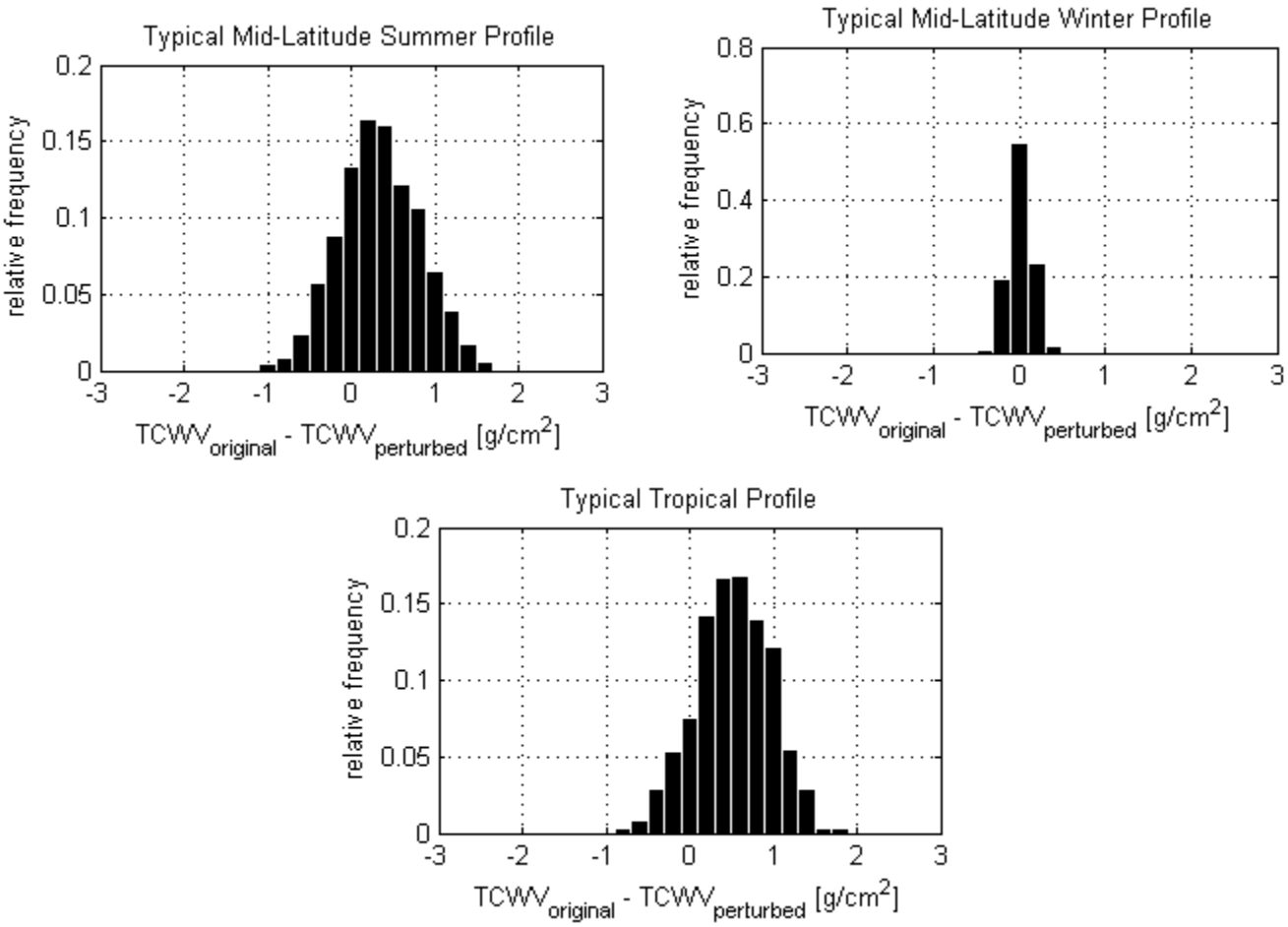

Figure 4.7 – Histograms of TCWV errors – difference between prescribed TCWV values and respective perturbations – for Mid-Latitude Summer (top), Mid-Latitude Winter (middle) and Tropical (bottom).

From Figure 4.7 it is possible to conclude that there is a shift to the right of the peak of TCWV perturbations, which tends to increase with TCWV.

For each profile (near 2000) of temperature and humidity a set of 1000 perturbed profiles are generated using the background error covariance matrix of the operational 4D-Var data assimilation scheme at ECMWF, and from those profiles 10 are randomly chosen to be used in the PMW and SMW algorithms.

4.5.4 Results

Results in this section respect to samples of, at least, 100 model runs and except when mentioned otherwise, the errors of LST are computed taking into account all perturbations.

The global RMSE of the PMW is 1.44 K, a value that is to be compared with the global RMSE of 1.63 K for the SMW. However it is worth subdividing the data in classes of TCWV and emissivity, as shown in Figures 4.8 and 4.9 for the distributions of land surface temperature versus the prescribed values of the same variable, for PMW and SMW, respectively. Both in PMW and SMW, the RMSE of estimated LST tends to increase with TCWV and with decreasing emissivity. The RMSE of LSTs as estimated with PMW ranges between about 0.6 K (for dry and high values of emissivity) to 2.5 K (for moist atmospheres). On the other hand, the results using SMW range from 0.9 K (for dry and high emissivity) to 2.6 K (for moist and lower emissivity values). The errors when using PMW are always lower than SMW, except for the class of moist atmosphere (4cm <= TCWV < 6cm) and high values of emissivity (>0.98), where the RMSE of estimated LST with PMW (with SMW) is of the order of 2.5 K (2.3 K).

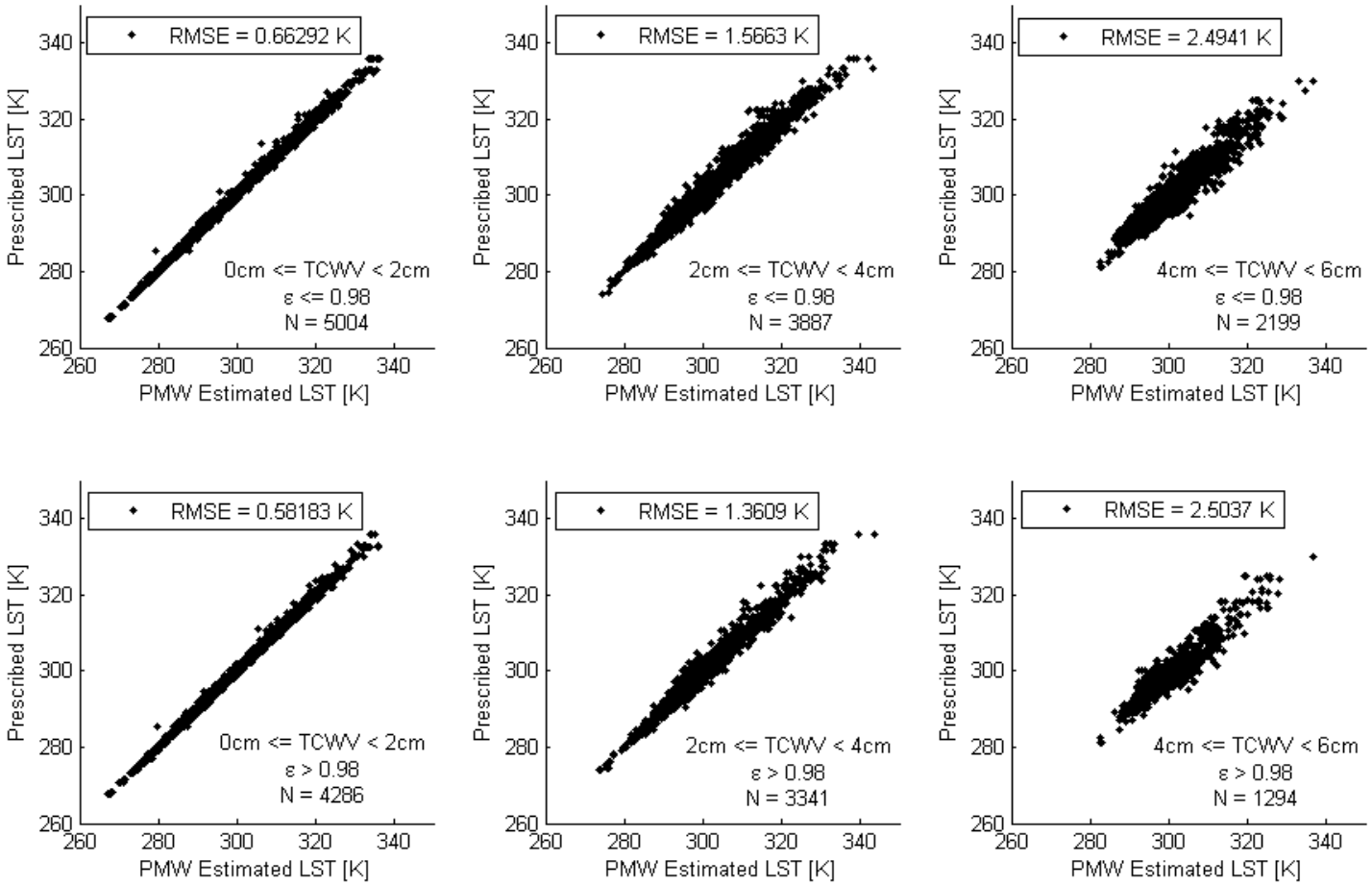

Figure 4.8 – Distribution of estimated LST using PMW algorithm – division in classes of TCWV and emissivity.

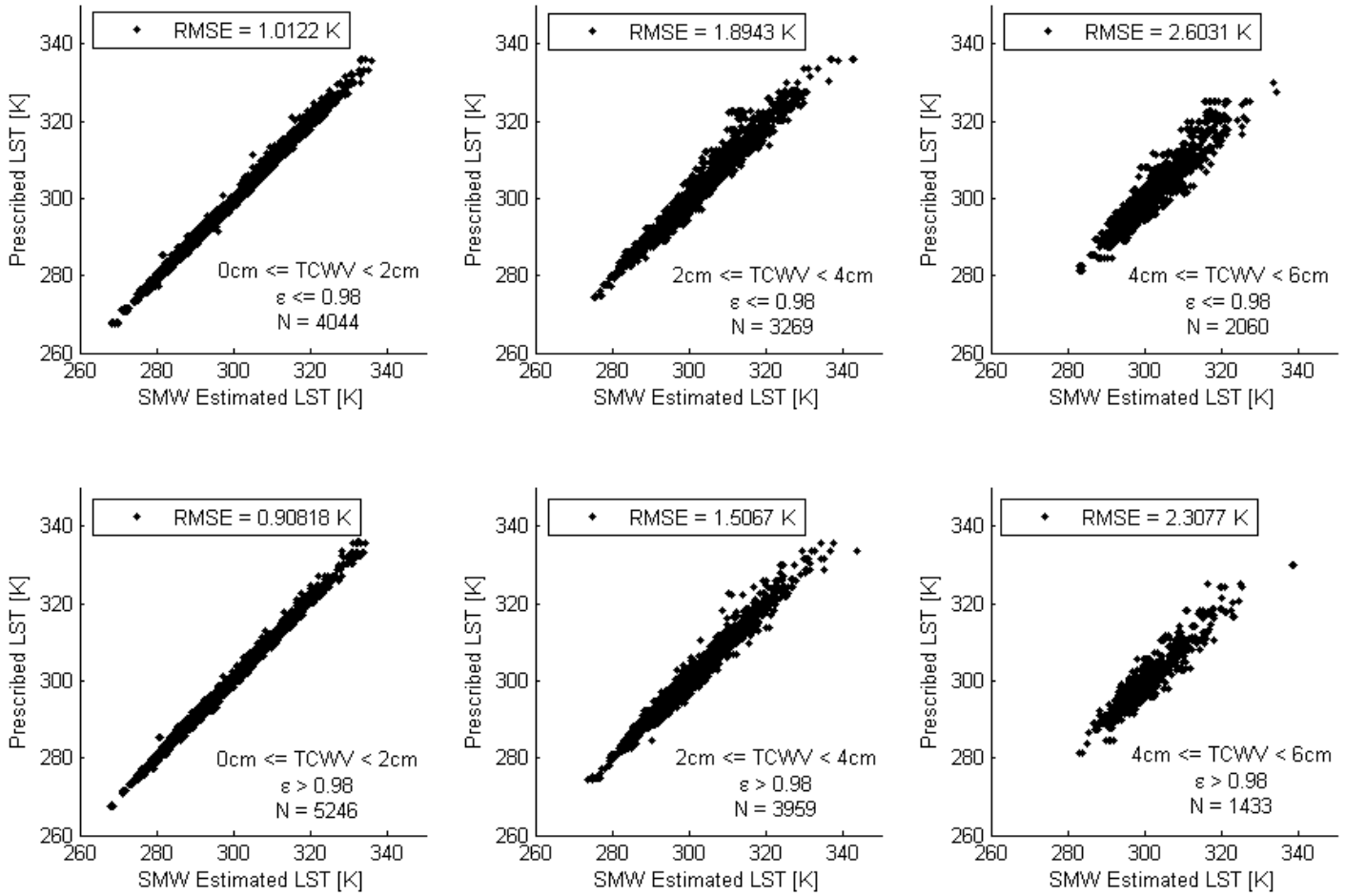

Figure 4.9 – Distribution of estimated LST using SMW algorithm – division in classes of TCWV and emissivity.

CHAPTER 5

5.1 CONCLUDING REMARKS

The main findings of this dissertation are addressed in Chapter 3 and 4. In Chapter 3 RTTOV and MODTRAN models are introduced and their performances compared, whereas in the Chapter 4 two approaches to retrieve LST using information in only one spectral infrared window are discussed: (1) a simple inversion of RTTOV using the RTE (see equation (2.24)), which was referred to as PMW; and (2) a statistical model which relates top-of-atmosphere radiances with LST, the so-called SMW.

From Figures 2.3 and 2.5 it may be concluded that there is a difference between the two radiative transfer models, which translates in the results obtained for transmittance: the RTTOV model tends to behave as a more transparent model than MODTRAN. Transmittance RMSE (bias) is 0.04 (0.03). The positive bias (see equation (2.3)) supports the above-mentioned conclusion, and the fact that RMSE and bias are in the same order leads to the conclusion that the "transparency" of RTTOV is a systematic deviation and not a random one. It may be further noted that a RMSE of 0.04 in transmittance may be relevant for dry atmospheres (an error from 10 to 20%). On the other hand brightness temperatures have a RMSE (bias) of 0.21 K (-0.04 K). In this case the errors seem to be randomly distributed and the RMSE represents a maximum of 0.1% of the temperature for cold atmospheres. These results suggest that RTTOV is in agreement with MODTRAN for the majority of cases, the exception being the most opaque atmospheres where the differences in transmittance may be relevant. Nevertheless the performance of RTTOV is still acceptable justifying its use in near real time applications, especially taking into consideration the much better performance of RTTOV in running times.

When comparing the two LST retrieval methods, i.e. using the PMW, and the SMW approaches for the dataset used of about 2000 profiles (extracted from dataset compiled by [13]), which were further perturbed in surface emissivity, temperature and humidity of profiles, and brightness temperatures according to the instrument noise, the RMSEs are of 1.44K and 1.63K, respectively. These results (considering all profiles as a whole with no class division) are very similar (with a difference of 0.19K) and below the threshold of 2K, which is the usually required threshold in LST accuracy. When dividing in classes of TCWV and emissivity (see Figures 3.8 and 3.9), PMW is always better, except in the class of moist atmospheres with high emissivity. Globally, the conclusion is that PMW is best suited to retrieve LST. However the need for RTE terms that are usually difficult to estimate, the simplicity of the SMW approach, and the closeness of obtained values of RMSE to those obtained with PMW make of SMW a very appealing approach for near real time estimations of LST.

5.2 FUTURE WORK

The LSA SAF is currently using a generalized split window algorithm (GSW) [25] to retrieve LST based on information in channels IR10.8 and IR12.0 as obtained from the SEVIRI instrument on-board Meteosat-10. Use of GSW is nevertheless impaired in the case of GOES and MTSAT imagers because information is only available in one TIR channel. In order to circumvent this problem, two algorithms have been introduced: the Dual-Algorithm (DA) which provides

estimation of LST from one MIR channel and one TIR channel; and the mono-channel algorithm that relies on a single TIR channel.

As described in [25], the mono-channel has the form

$$LST = aT_b + b + \Delta LST \tag{5.1}$$

where ΔLST is the model error and a, b are the model coefficients.

A statistical mono-window (SMW) algorithm, similar to the one given by Equation (5.1) was developed in the present dissertation based on a large set of simulations generated by RTTOV. It is anticipated that this algorithm will be the basis for a new operational LST product based on GOES and MTSAT developed within the context of Copernicus Global Land Service [25].

Results from this dissertation demonstrate that RTTOV is a useful and computationally efficient tool to develop algorithms to estimate LST from information on a single TIR window from a variety of sensors on-board geostationary satellites.

This may be achieved by using procedures similar to those followed in this dissertation, where RTTOV was applied to a very large dataset of atmospheric profiles and surface types. Retrieval of LST may then be achieved by using a "physical" mono window where RTTOV is used to solve the RTE. An alternate procedure consists in developing statistical mono-channel algorithms where regression coefficients are estimated using simulations by RTTOV. As already mentioned, results obtained in this dissertation from perturbation analysis suggest that "physical" approaches tend to perform slightly better than statistical ones, but the latter approach leads to better results in case of wet atmospheres associated to high values of surface emissivity. This aspect deserves to be further investigated.

REFERENCES

[1] Trigo, I.F., Viterbo, P., 2003. Clear-sky window channel radiances: A comparison between observations and the ECMWF model. J. Appl. Meteorol., vol. 42, no. 10, pp. 1463–1479.

[2] Qin, J., Liang, S., Liu, R., Zhang H., Hu, B., 2007. A weak-constraint-based data assimilation scheme for estimating surface turbulent fluxes. IEEE Geosci. Remote Sens. Lett., vol. 4, no. 4, pp. 649–653.

[3] Kustas, W.P., Norman, J.M., 1996. Use of remote sensing for evapotranspiration monitoring over land surfaces. Hydrol. Sci. J., vol. 41, no. 4, pp. 495–515.

[4] Jin, M., 2004. Analysis of land skin temperature using AVHRR observations. Bull. Amer. Meteorol. Soc., vol. 85, no. 4, pp. 587–600.

[5] Yu, Y., Privette, J.L., Pinheiro A.C., 2008. Evaluation of split-window land surface temperature algorithms for generating climate data records. IEEE Trans. Geosci. Remote Sens., vol. 46, no. 1, pp. 179–192.

[6] Hocking, J., Rayer, P., Saunders, R. Matricardi, M., Geer, A., Brunel, P. (2011). RTTOV v10 Users Guide. Met Office, Exeter, UK; ECMWF; Météo France.

[7] Schott, J.R. (2007). *Remote Sensing: The Image Chain Approach.* Second Edition. Oxford: University Press.

[8] Byrnes, J., 2009. *Unexplored Ordnance Detection and Mitigation.* Springer, pp. 21–22. ISBN 978-1-4020-9252-7.

[9] Peixoto, J.P., Oort, A.H. (1992). *Physics of Climate.* First Edition. New York: Springer.

[10] Bohren, C.F., Clothiaux, E. (2006). *Fundamentals of Atmospheric Radiation.* First Edition. Weinheim: Wiley-VCH.

[11] Cantor, G., 2004. Oxford Dictionary of National Biography (DNB): Young, Thomas.

[12] Kneizys, F. X., Abreu, L. W., Anderson, G. P., Chetwynd, J. H., Shettle, E. P., Berk, A., Bernstein, L. S., Robertson, D. C., Acharya, P., Rothman, L. S., Selby, J. E. A., Gallery, W. O., Clough, S. A. (1996). The MODTRAN 2/3 Report and LOWTRAN 7 Model.

[13] Borbas, S.W. Seemann, H.-L. Huang, J. Li, andW. P. Menzel, "Global profile training database for satellite regression retrievals with estimates of skin temperature and emissivity," in Proc. Int. ATOVS Study Conf.-XIV, Beijing, China, May 25–31, 2005, pp. 763–770.

[14] Qin, Z., Karnieli, A., Berliner, P. (2001). A mono-window algorithm for retrieving land surface temperature from Landsat TM data and its application to the Israel–Egypt border region. International Journal of Remote Sensing, 22(18), 3719–3746.

[15] Jiménez-Munõz, J. C., Sobrino, J. A. (2003). A generalized single-channel method for retrieving land surface temperature from remote sensing data. Journal of Geophysical Research, 108 (doi: 10.1029/2003JD003480).

[16] Sobrino, J. A., Jiménez-Munõz, J. C., Paolini, L. (2004). Land surface temperature retrieval from LANDSAT TM 5. Remote Sensing of Environment, 90, 434 – 440.

[17] Wan, Z., Dozier, J. (1989). Land-Surface Temperature Measurement from Space: Physical Principles and Inverse Modeling. *IEEE Transactions on Geoscience and Remote Sensing, 27*, 268 – 278.

[18] Yu, Y., Privette, J.L. (2008). Evaluation of Split-Window Land Surface Temperature Algorithms for Generating Climate Data Records. *IEEE Transactions on Geoscience and Remote Sensing, 46*, 179 – 192.

[19] Wan, Z., Dozier, J. (1996). A Generalized Split-Window Algorithm for Retrieving Land-Surface Temperature from Space. *IEEE Transactions on Geoscience and Remote Sensing*, 34, 892 – 905.

[20] Peres, L.F., DaCamara, C.C. (2004). Land surfasse temperature and emissivity estimation based on the two-temperature method: sensitivity analysis using simulated MSG/SEVIRI data. *Remote Sensing of Environment, 91*, 377 – 389.

[21] Goel, N. S., Sterbel, D. E. (1983). Inversion of vegetation canopy reflectance models for estimation agronomic variables: I. Problem definition and initial results using Suit's model. *Remote Sensing of Environment, 39*, 255– 293.

[22] EUMETSAT (2007). A planned Change to the MSG Level 1.5 Image Product Radiance Definition. EUM/OPS-MSG/TEN/06/0519.

[23] Freitas, S.C., Trigo, I.F., Bioucas-Dias, J.M., Göttsche, F-M. (2010). Quantifying the Uncertainty of Land Surface Teperature Retrievals From SEVIRI/Meteosat. *IEEE Transactions on Geoscience and Remote Sensing, 48*, 523 – 534.

[24] Dereniowski, D., Kubale, M. (2004). Cholesky Factorization of Matrices in Parallel and Ranking of Graphs. 5th International Conference on Parallel Processing and Applied Mathematics. Lecture Notes on Computer Science 3019. Springer-Verlag. pp. 985–992. doi:10.1007/978-3-540-24669-5_127. ISBN 978-3-540-21946-0.

[25] Trigo, I., Freitas, S., Perdigão, R., Barroso, C., Macedo, J., 2010. Algorithm Theoretical Basis Document (ATBD), Land Surface Temperature, Geoland 2.